Drug Design and Optimisation at the Dihydroorotate Dehydrogenase Receptor using the Teriflunomide Scaffold as a Lead.

Submitted in partial fulfilment

of the requirements of the

Degree of Master of Pharmacy

Paula Zammit

Department of Pharmacy

2025

Abstract

Dravet Syndrome is a dangerous form of childhood epilepsy, for which current anti-epileptic treatment is insufficient. Animal studies show that intracerebral dihydroorotate dehydrogenase (DHODH) inhibition is a novel route for the treatment of epilepsy. Teriflunomide has been identified as a potent inhibitor of DHODH, with poor blood brain barrier (BBB) permeation due to its high polarity.

The aim of this study was to identify high *in silico* binding affinity DHODH inhibitors based on the teriflunomide scaffold, which are orally bioavailable and have improved non-polar characteristics, predisposing them to increased intra-cerebral penetration. The virtual screening and *de novo* drug design methods were applied.

PDB crystallographic depositions 1D3H and 3U2O, describing the bound coordinates of the *holo* DHODH receptor with ligands teriflunomide and its biaryl analogue, respectively, were used to create a consensus pharmacophore. Pharmacophore-based virtual screening was carried out in ZINCPharmer®, with application of the Rule of 3 for lead-likeness. The resultant molecules were filtered in MONA® for drug-likeness, generating a cohort of 299 Lipinski Rule compliant molecules. Ranking of the molecules according to their binding affinity for the protomol, generated in SYBYL-X®, and lipophilicity, lead to the identification of high affinity molecules capable of penetrating the BBB.

The ‘pocket’ module of LigBuilder® was used to elucidate the DHODH ligand binding pocket, as delineated around the bioactive conformation of teriflunomide. Structure activity relationship (SAR) data from X-Score® and a 2D topology map of the interactions between teriflunomide and the cognate receptor DHODH, guided the creation of seed structures which

sustained molecular growth within the DHODH ligand binding pocket at pre-defined *loci*. The resultant molecules were filtered for Lipinski Rule compliance and ranked according to binding affinity for the DHODH ligand binding pocket and lipophilicity. Six teriflunomide analogues, with a propensity to oral bioavailability and intracerebral penetration were identified. 2D topology maps describing the molecular interactions they forge with the DHODH receptor were created to determine their binding modalities.

The preliminary cohort of molecules produced will be used in iterative rounds of rational drug design, with optimisation carried out to improve their toxicity profile and to further explore the defined pharmacophoric space.

Acknowledgements

I would like to thank my supervisor Dr Claire Shoemake and the Department of Pharmacy for their guidance and for the knowledge imparted throughout the Pharmacy programme.

To my family and friends- thank you for always being there for me.

Table of Contents

List of Tables

List of Figures

List of Appendices

List of Abbreviations

AEDs	Anti-Epileptic Drugs
ADMET	Absorption, Distribution, Metabolism, Excretion and Toxicity
AI	Artificial Intelligence
BBB	Blood Brain Barrier
clogP	Calculated logarithm of the partition coefficient between n-octanol and water
DHODH	Dihydroorotate Dehydrogenase
FMN	Flavin Mononucleotide
LD_{50}	Median Lethal Dose
PAINs	Pan Assay Interference Compounds
PDB	Protein Data Bank
SAR	Structure Activity Relationships
SMILES	Simplified Molecular Input Line Entry System
RMSD	Root Mean Square Distance
2D	2-Dimensional
3D	3-Dimensional

Chapter 1

Introduction

1.1 Dravet Syndrome

Dravet Syndrome is a rare but severe form of epilepsy which is genetically inherited. Its characteristics include prolonged frequent seizures, developmental delays and speech and motor impairment (Rosander & Hallböök, 2015). It usually presents within the first year of life, with the non-epileptic symptoms presenting as the child grows up (Zuberi *et al.*, 2022). The epileptic seizures can be febrile, afebrile, generalised clonic or hemiclonic and may be triggered by an elevation of body temperature. They are resistant to anti-epileptic drugs (AEDs) and may progress to a *status epilepticus*, if recurring in clusters (Mei *et al.*, 2019).

The incidence of Dravet Syndrome is 1 in 14,000 in the US (Wu *et al.*, 2015). 70% to 80% of these patients have mutations and deletions in the SCN1A gene (α_1-subunit of the sodium channel) of chromosome 2q, most of which are paternally inherited (Rosander & Hallböök, 2015; Mei *et al.*, 2019). Premature mortality affects up to 21% of patients (Shmuely *et al.*, 2016) and most patients suffer from intellectual disability and gait disorders. Episodes of *status epilepticus* may worsen developmental regression (Zuberi *et al.*, 2022).

1.2 Current Treatment Options for Dravet Syndrome

The treatment aims for Dravet Syndrome are the reduction of seizure frequency, ending prolonged convulsions and minimising the side effects of treatment. Pharmacotherapy is often complex and requires regular adjustments. It is only partially effective and, in some cases, ineffective, leading to aggravated seizures, a higher risk of *status epilepticus* and a worsened cognitive outcome. First-line treatment is sodium valproate, which often presents with side-effects since high serum concentrations are required to attain a pharmacological effect (Wirrell *et al.*, 2017; von Spiczak & Stephani, 2019).

Second-line treatment for Dravet syndrome includes clobazam and the addition of stiripentol as an adjunct (Wirrell *et al.*, 2017; Ziobro *et al.*, 2018). Stiripentol has been shown to significantly decrease the frequency of seizures, however the effect is less pronounced if the drug is initiated after the age of two (Wheless & Weatherspoon, 2025). Ketogenic diets are also considered as a safe second-line treatment option for Dravet syndrome which has not been adequately controlled by three or four AEDs (Wirrell *et al.*, 2017; Cross *et al.*, 2019). However, longterm adherence to a ketogenic diet is often challenging and randomised controlled trials are lacking (Li *et al.*, 2025).

Recent adjunctive therapies approved for Dravet syndrome include fenfluramine and cannabidiol. Fenfluramine has fewer sedative side effects and reduces hospitalisations. Nonetheless, it decreases body mass index, requiring growth monitoring and nutritional support, especially in paediatric populations (Boncristiano *et al.*, 2025). Cannabidiol was shown to stabilise or reduce the number of concomitant AEDs used, thereby decreasing treatment and side effect burden. Discontinuation rates of cannabidiol are considerable, being reported to be as high as 26 % (Eltze *et al.*, 2025). Other commonly used antiepileptic drugs, such as the sodium channel blockers lamotrigine and phenytoin, worsen seizures in Dravet syndrome (Knupp & Wirrell, 2018).

1.3 Structure of the human DHODH enzyme

There are two classes of human DHODH enzymes, namely cytosolic DHODH and mitochondrial DHODH, the latter being the target of this study. Mitochondrial human DHODH consists of a large C-terminal domain, also known as the catalytic domain, and a small N-terminal domain, also known as the membrane bound domain. The two domains are

linked by an extended loop. The C-terminal domain is an α-β barrel structure which contains the active site of the enzyme. It is intrinsically flexible, allowing for the binding of structurally diverse DHODH inhibitors (Zeng *et al.*, 2019). The α-β barrel consists of a central barrel comprised of eight parallel β strands which are surrounded by eight α-helices. A subdomain consisting of loops and secondary structural elements is found on the top of the barrel. The bottom of the barrel is composed of two N-terminal antiparallel β strands. The C-terminal contains a binding site to which flavin mononucleotide (FMN) and dihydroorotate substrate bind to undergo a redox reaction (Reis *et al.*, 2017).

The N-terminal domain is an α-helical structure consisting of approximately forty residues which fold into two α-helices and which are linked by a short loop. The two α-helices form a tunnel that ends in the cavity where FMN binds, allowing for co-factor ubiquinone to enter the tunnel to undergo a redox reaction with FMN. The tunnel is also the binding site for DHODH inhibitors. The N-terminus of the protein contains the mitochondrial localisation signal and a hydrophobic sequence that anchors the protein to the membrane(Popova, 2020; Zuo *et al.*, 2020).

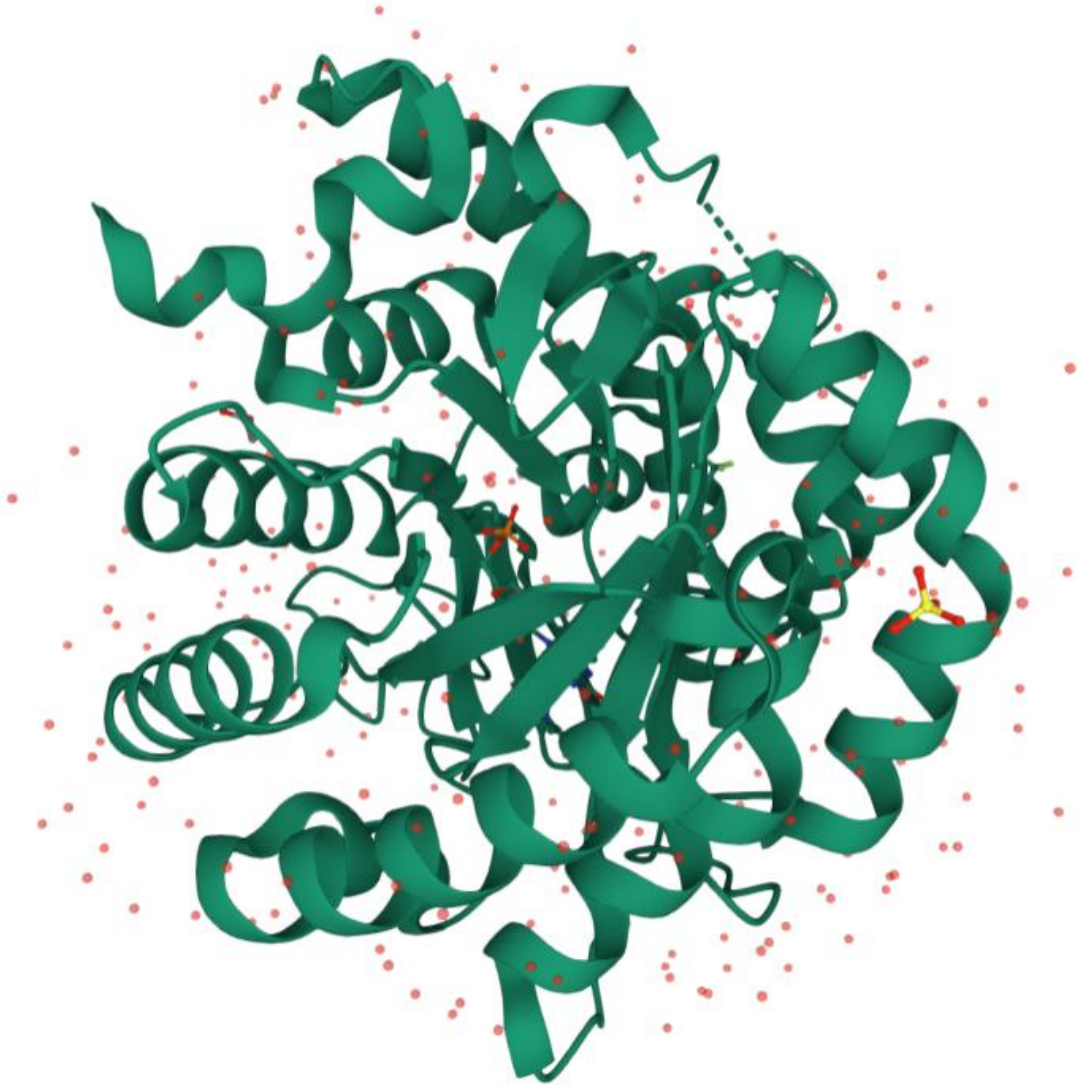

Figure 1.1 Protein Data Bank (PDB) crystallographic deposition 1D3H describing the bound coordinates of the DHODH receptor and antiproliferative agent A771726 (teriflunomide). Adapted from: Liu S, Neidhardt E, Grossman T, Ocain T, Clardy J. Structures of human dihydroorotate dehydrogenase in complex with antiproliferative agents. Structure. 2000;8(1):25-33. doi: 10.1016/s0969-2126(00)00077-0.

1.4 Therapeutic implications of DHODH inhibition

The inhibition of DHODH is already being exploited in the treatment of autoimmune disease. Leflunomide is licenced for the treatment of rheumatoid arthritis, where DHODH inhibition

suppresses the response of cells to cytokines and the production of antibodies (Alamri *et al.*, 2021). In malignant disease, DHODH is being investigated as a potential therapeutic target, since pyrimidine synthesis, which is carried out by DHODH, has a role in tumour cell proliferation. Already existing DHODH inhibitors, such as brequinar, teriflunomide and leflunomide, together with novel DHODH inhibitors, are being tested in leukaemia, colorectal cancer and breast cancer (Zhou *et al.*, 2021). In malaria, triazolopyrimidine based DHODH inhibitors have shown promising results as they are highly selective to *Plasmodium falciparum* DHODH (Singh *et al.*, 2017).

1.5 Role of DHODH inhibition in epilepsy

DHODH is a mitochondrial enzyme located in the inner mitochondrial membrane. It is involved in the mitochondrial electron transport chain and in *de novo* pyrimidine biosynthesis. In neurons, mitochondria regulate the setpoint of neuronal activity, of which DHODH is a key regulator. This was hypothesised by Styr *et al* (2019), by means of DHODH inhibition using teriflunomide. The two main mechanisms by which the neuronal setpoint was regulated were by facilitation of activity dependent mitochondrial calcium buffering and by a decrease in the spare respiratory capacity of mitochondria. Both alter the excitatory to inhibitory neuronal ratio and reversibly decrease the spontaneous neuronal mean firing rate. Glutamate release was also decreased by teriflunomide induced DHODH inhibition, which resulted in reduced excitatory synaptic transmission and contributed to maintaining the new mean firing set point of neurones. Taken together, these effects decrease the susceptibility to seizures, making DHODH a promising target in the treatment of epilepsy (Styr *et al.*, 2019; Uytterhoeven *et al.*, 2019).

1.6 Teriflunomide

Teriflunomide is the active metabolite of leflunomide. It is an immunosuppressive drug indicated in rheumatoid arthritis and multiple sclerosis. The molecular mass of teriflunomide is 270.2 Daltons and its calculated logarithm of the partition coefficient between n-octanol and water (clogP) is 2.140 (Liu *et al.*, 2000). It has two hydrogen bond donors and six hydrogen bond acceptors.[1] Teriflunomide is absorbed completely and rapidly after oral administration and has a low volume of distribution as it binds extensively to plasma proteins (Rouini *et al.*, 2020).

Mouse studies have shown that if injected into brain, teriflunomide significantly reduces the severity of epileptic seizures, however, oral teriflunomide cannot reach cerebral tissue to exert an anti-epileptic effect as it poorly penetrates the BBB.[2] This is the result of teriflunomide's low volume of distribution and its high affinity to the membrane efflux transport breast cancer resistance protein, which is abundantly expressed on the endothelial cells of the BBB (Rzagalinski *et al.*, 2019). Therefore, novel AEDs, effective in Dravet Syndrome must necessarily be non-polar analogues of teriflunomide which can cross the BBB.[2]

[1] National Library of Medicine (NLM). PubChem Compound Summary for CID 54684141, Teriflunomide [Internet]. Maryland (USA): NLM; 2025 [cited 2025 Jul 23]. Available from: https://pubchem.ncbi.nlm.nih.gov/compound/54684141.

[2] Laboratory Equipment. Study Paves Way for Innovative Treatment for Epilepsy [Internet]. South San Francisco (United States): Laboratory Equipemtn;2019 [cited 2025 Jul 15. Available from: https://www.proquest.com/docview/2220074565/fulltext/F93C3271766748A6PQ/1?accountid=27934.

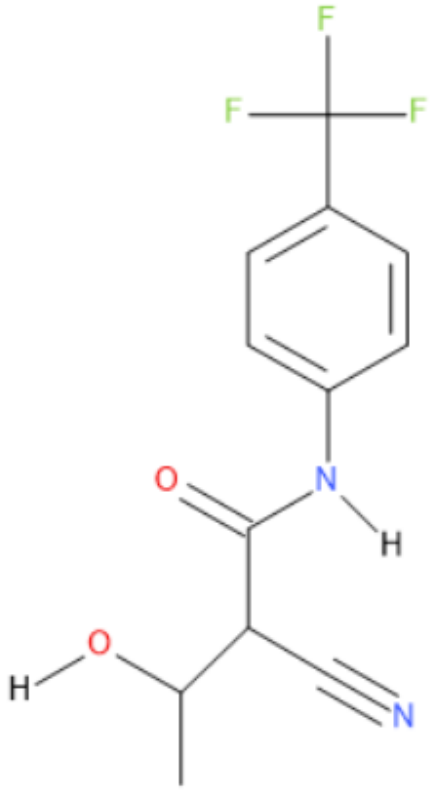

Figure 1.2 2-Dimensional (2D) structure of teriflunomide rendered using Biovia Draw®.[3]

1.7 Interactions of teriflunomide with the DHODH receptor

Teriflunomide displaces ubiquinone from its ligand binding site within the hydrophobic channel of the DHODH receptor. There it forms critical interactions with key binding site residues Tyr^{356} and Arg^{136}. The enolic hydroxyl group forms a direct interaction with Tyr^{356} whereas with the other key binding site residue, the interactions formed are water-mediated hydrogen bonds. Arg^{136} interacts with the carbonyl oxygen of teriflunomide. As the

[3]Dassault Systèmes: Biovia Draw®. Version 21.1 [software]. Dassault Systèmes. 2024 [cited 2025 Jul 26; downloaded 2023 Oct 19]. Available from: https://discover.3ds.com/biovia-draw-academic#_ga=2.9885366.2038323275.1652726867-4a55e360-cfd1-11ec-9db0-078235bac709

hydrophobic channel within which teriflunomide binds with the receptor ends in the FMN binding site, redox reactions can occur. Additionally, hydrophobic contacts exist between the 4-trifluoromethylphenyl moiety and the DHODH receptor (Munier-Lehmann *et al.*, 2013; Kujawski *et al.*, 2015).

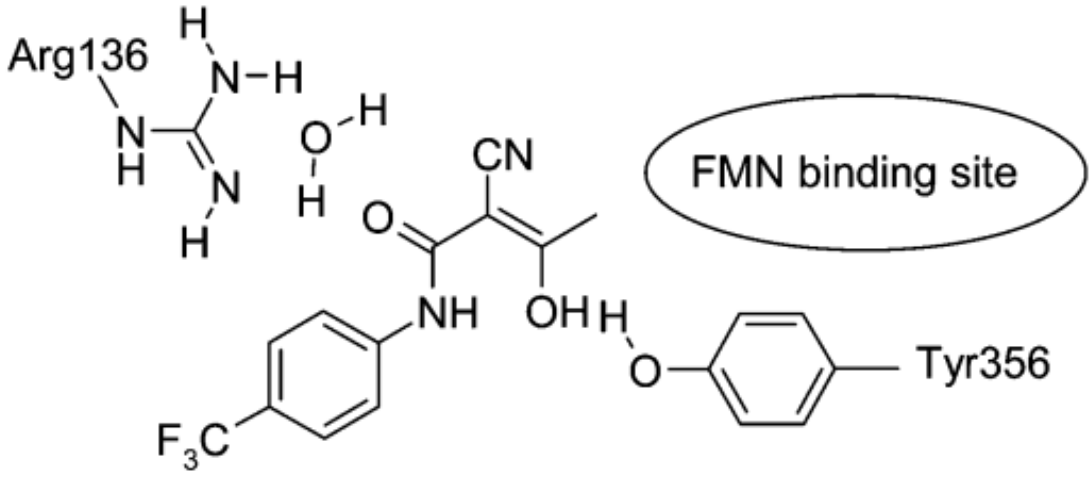

Figure 1.3 Critical interactions forged between teriflunomide and the DHODH receptor. Reproduced from: Munier-Lehmann H, Vidalain P, Tangy F, Janin Y. On Dihydroorotate Dehydrogenases and Their Inhibitors and Uses. Journal of Medicinal Chemistry. 2013;56(8):3148-3167. doi: 10.1021/jm301848w

1.8 Existing DHODH inhibitors based on the teriflunomide scaffold

There is little evidence in the literature about the existence of teriflunomide-based DHODH inhibitors for the management of epilepsy. However, studies have been carried out to develop DHODH inhibitors for other diseases. Li *et al.* (2022) used SAR data to design a series of orally active teriflunomide derivatives for the treatment of colorectal cancer. They determined that a fluorine atom and hydrophobic side chain on the phenyl moiety of teriflunomide increase DHODH inhibitory activity. Compound A37 exhibited potent DHODH activity and demonstrated an acceptable oral safety profile. However, further study

is required to ascertain whether its clogP value, which was not calculated in the study, is high enough to allow the compound to penetrate the BBB. Consequently, the compound could be tested for its potential anti-epileptic effects.

Similarly, Nada *et al.* (2023) developed a series of DHODH inhibitors for lung cancer using virtual screening. The molecules designed were based on a hybrid scaffold of leflunomide (the prodrug of teriflunomide), LCG-A37 and GSK983, which are potent DHODH inhibitors. The functional groups trifluoromethyl and the amide linker of leflunomide were used to create the hybrid scaffold as they impart steric and electronegative effects and have an important role in hydrogen bond formation, respectively. For the compounds created, no clogP values were provided.

1.9 Brain permeable DHODH inhibitors

In 2025, a patent application (WO 2025/041128) was submitted by Pessah *et al.* (2025) for DHODH inhibitors which cross the BBB, for use in Alzheimer's disease and epilepsy. The compounds created were determined to have an anti-convulsant effect in *in vivo* studies carried out in mice and in the Dravet syndrome zebrafish larvae model. When administered orally, Compound SLN-031 was well absorbed and penetrated in the BBB in sufficient concentrations to decrease seizure susceptibility in mouse epilepsy models (Pessah *et al.*, 2025). Compound SLN-031 shows some structural similarities to teriflunomide, namely a fluorinated phenyl moiety and a linking amide group.

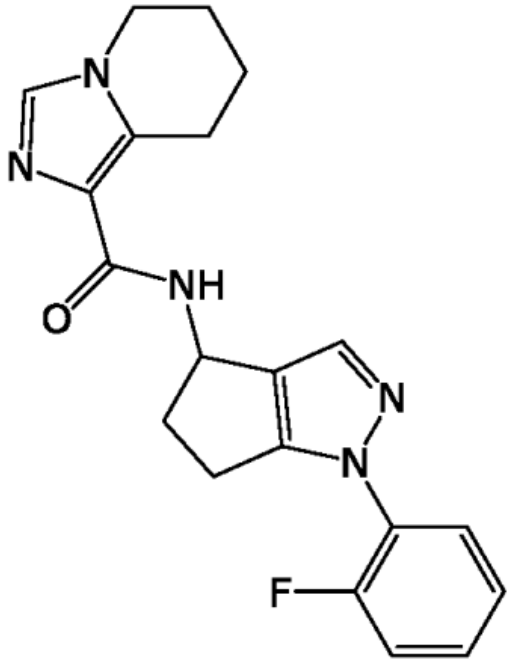

Figure 1.4 Strucutre of Compound SLN-031. Reproduced from: Pessah N, Getter T, Mostinski Y, Bingor A, Paker-Krush Y, Roussay-Maggi C, inventors; Selene Therapeutics Ltd., assignee. Brain Permeable DHODH Inhibitors and Uses Thereof. World Intellectual Property Organisation patent WO2025041128A1. 2025 Feb 27.

1.10 Rational Drug Design

Rational drug design involves a thorough understanding of the target protein structure. Protein design algorithms have been developed to calculate how proteins fold and catalyse in their most suitable conformational state (Tiwari *et al.*, 2012). Virtual screening is a rational drug design approach which aims to reduce the number of candidate molecules sent for *in vitro* testing by rapidly searching large databases of existing or synthesisable compounds (Ripphausen *et al.*, 2011). Conversely, *de novo* drug design involves the independent design of a compound at the chosen target site, taking into consideration critical interaction points which elicit the desired response in the target (Rosales-Hernández & Correa-Basurto, 2015).

1.11 Software

The following software were used in the study.

1.11.1 BIOVIA Discovery Studio Visualizer® v. 24.1.0.23298

This molecular modelling software can be used to simulate and visualise small molecules and macromolecules. It can create 2D and 3 dimensional (3D) images of receptor-ligand complexes, to depict the molecular interactions in place.[4]

1.11.2 BIOVIA Draw® v.21.1

This program allows the user to draw 2D chemical structures and reactions.[3]

1.11.3 LigBuilder® v1.2

LigBuilder® was designed for structure-based *de novo* drug design and optimisation. It identifies a protein's ligand binding pocket and estimates its drugability. Using its 'build' and 'link' modules, novel ligands can be generated (Wang *et al.*, 2000).

1.11.4 LigandScout® v.4.4

This program can be used to create pharmacophores and determine the physicochemical properties of ligands, along with their interactions within the ligand binding pocket of a receptor (Wolber & Langer, 2005).

---

[3] Dassault Systèmes. Biovia Draw®. Version 21.1 [software]. Dassault Systèmes. 2024 [cited 2025 Jul 26; downloaded 2023 Oct 19]. Available from: https://discover.3ds.com/biovia-draw-academic#_ga=2.9885366.2038323275.1652726867-4a55e360-cfd1-11ec-9db0-078235bac709.

[4] Dassault Systèmes. Biovia Discovery Studio Visualizer®. Version 24.1.0.23298 [software]. Dassault Systèmes. 2025 [cited 2025 Jul 25; downloaded 2024 Jan 16]. Available from: https://discover.3ds.com/discovery-studio-visualizer-download.

1.11.5 MONA®

MONA® is a cheminformatics tool designed to process large datasets of small molecules. It can be used to sort out duplicate molecules and sort molecules by their physicochemical properties (Hilbig & Rarey, 2015).

1.11.6 Pro-Tox-3.0®

Pro-Tox 3.0® is an open access computational platform into which a 2D chemical structure can be read to generate a toxicological profile for the compound. It uses molecular similarities and machine learning models to predict a variety of toxicological endpoints (Banerjee *et al.*, 2024).

1.11.7 SwissADME®

SwissADME® is an open access web tool which analyses the pharmacokinetics, physicochemical properties and drug-likeness of chemical structures (Daina *et al.*, 2017).

1.11.8 SYBYL-X® v.2.1.1

This program can be used to model and simulate small molecules and macromolecules such as receptors. Small molecules can be docked into receptors to calculate their binding affinities (Ash *et al.*, 2010).

1.11.9 X-Score® v.1.3

This program calculates the binding affinities for protein ligand complexes. It can also be used in structure-based drug design to identify which parts of a ligand are contributing to the binding affinity, for the ligand to be optimised accordingly (Wang *et al.*, 2002).

1.11.10 VMD®

VMD® is a molecular dynamics program which visualises structures in a variety of rendering styles. Molecular dynamics simulations can also be analysed (Humphrey *et al.*, 1996).

1.11.11 ZINCPharmer®

ZINCPharmer® is an open access resource used for virtual screening. Using a pharmacophore, it retrieves molecules from large databases of synthesisable molecules. Various filters can be applied to obtain a cohort of molecules with the desired characteristics (Koes & Camacho, 2012).

1.12 Rationale of the study

Despite the numerous AEDs on the market, many patients are not seizure-free, particularly if suffering from refractory forms of epilepsy such as Dravet syndrome. Consequently, new AEDs with mechanisms of action differing from those of licensed AEDs are required. To date, no DHODH inhibitors have been licensed for use in epilepsy. Since teriflunomide is a potent DHODH inhibitor which reduces the frequency of seizures when administered intracerebrally, the development of orally bioavailable teriflunomide analogues capable of penetrating the BBB may lead to the identification of viable compounds, resulting in the development of a novel class of AEDs.

1.13 Aims and Objectives of the study

The scope of the study was to develop orally available analogues of teriflunomide capable of crossing the BBB to inhibit intracerebral DHODH. This was achieved by means of two distinct *in silico* drug design approaches, namely virtual screening and *de novo* drug design.

Lipinski's Rule of 5 (Lipinski *et al.*, 1996) and the Rule of 3 (Congreve *et al.*, 2003) with respect to rotatable bonds were applied and molecules with a clogP higher than that of teriflunomide were selected, in order to generate a preliminary cohort of novel DHODH inhibitors for further optimisation studies.

Chapter 2

Methodology

2.1 Overview

The *in-silico* study was divided into two main phases, namely virtual screening and *de novo* drug design. Two approaches were used since the former retrieves pre-existing structures based on pharmacophores, whereas the latter makes use of the 3D structure of the target receptor to generate novel molecules based on seed structures (Lin *et al.*, 2020) . Both aimed to develop teriflunomide analogues which are capable of modulating the target DHODH receptor within the brain, as this alters the mean firing set point of neurons, decreasing the susceptibility to seizures (Styr *et al.*, 2019).

2.2 Selection of PDB Crystallographic Depositions

PDB crystallographic deposition 1D3H describing the bound coordinates of the human DHODH receptor complexed with antiproliferative agent A771726 (teriflunomide) (Liu *et al.*, 2000) and PDB crystallographic deposition 3U2O describing the bound coordinates of the human DHODH receptor complexed with a small molecule inhibitor (methyl 4-{[(2Z)-2-cyano-3-hydroxypent-2-enoyl]amino}-4'-fluorobiphenyl-2-carboxylate- a biaryl analogue of teriflunomide) (Erra *et al.*, 2011), were identified.

PDB crystallographic deposition 1D3H is resolved to 1.80 Angstroms using X-Ray diffraction, indicating that the crystal structure of the teriflunomide-DHODH receptor complexation is highly resolved, and that the location of each atom has been predicted with high confidence. The quality of the crystallographic model compared to simulated models is also high since the R-value and the R value observed are similar, being 0.162 and 0.185 respectively, with a perfect fit having an R-value of 0. The ligand quality of teriflunomide is ranked as ‘better’ with regards to experimental data fitting but ‘worse’ with regards to

geometry, indicating that geometrical parameters such as bond angles and lengths are not considered to be particularly accurate (Liu *et al.*, 2000).

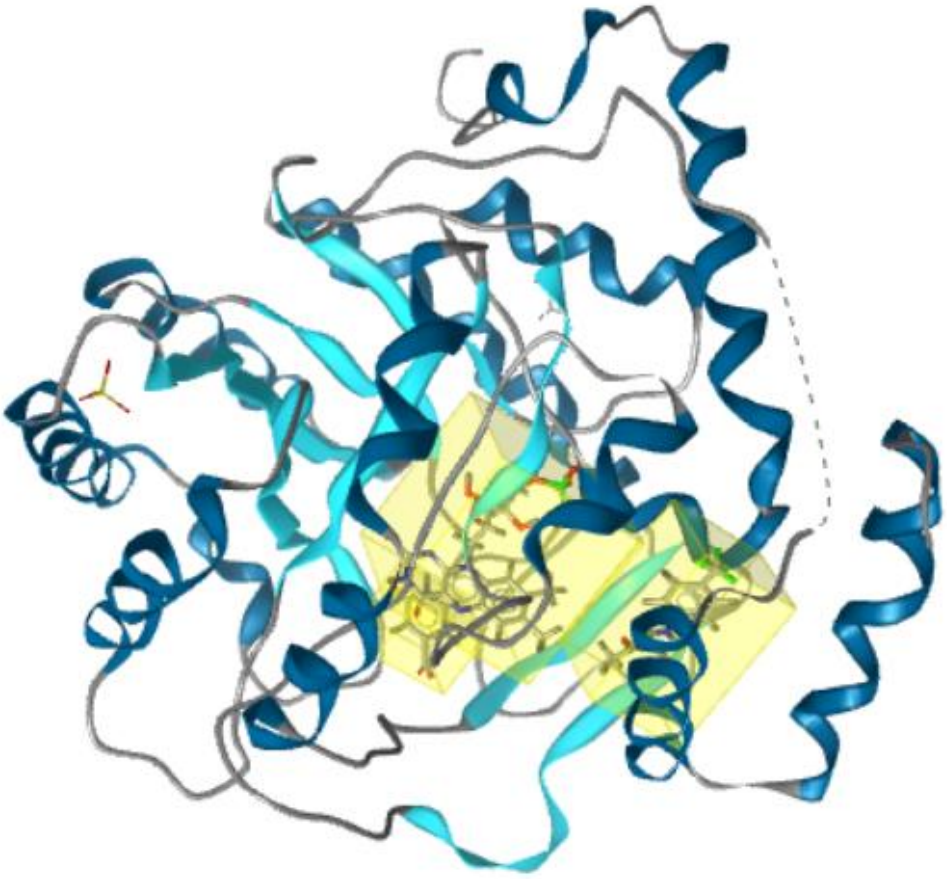

Figure 2.1 PDB crystallographic deposition 1D3H (Liu *et al.*, 2000) describing the bound coordinates of human DHODH receptor and antiproliferative agent A771726 (teriflunomide), as rendered in LigandScout® (Wolber & Langer, 2005).

PDB crystallographic deposition 3U2O is resolved to 2.18 Angstroms using X-Ray diffraction, indicating that the crystal structure has not been resolved as well as that of PDB crystallographic deposition 1D3H. However the ligand quality of the biaryl analogue of

teriflunomide is better than that of teriflunomide, most notably with respect to geometry (Erra *et al.*, 2011).

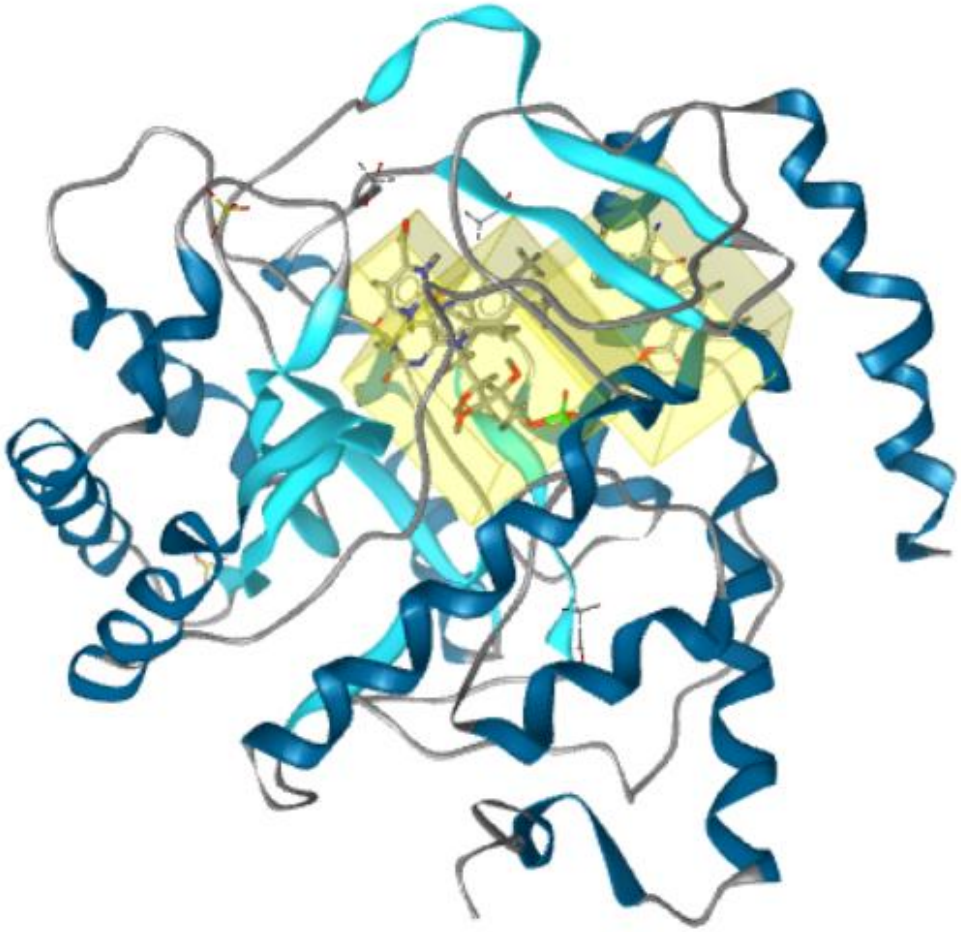

Figure 2.2 PDB crystallographic deposition 3U2O (Erra *et al.,* 2011) describing the bound coordinates of human DHODH receptor and a small molecule inhibitor (a biaryl analogue of teriflunomide), as rendered in LigandScout® (Wolber & Langer, 2005).

PDB crystallographic deposition 3U2O was selected since its ligand, a biaryl analogue of teriflunomide, is a potent inhibitor of DHODH which is orally bioavailable. It has an improved pharmacokinetic profile since its half-life is shorter than that of teriflunomide.

Compared to teriflunomide, it also contains an additional fluorophenyl group which has increased interactions with the hydrophobic region of the DHODH ligand binding pocket (Erra *et al.*, 2011).

2.3 Virtual Screening

2.3.1 Overview of Virtual Screening

Figure 2.3 shows a flow chart of the study design followed during the virtual screening phase.

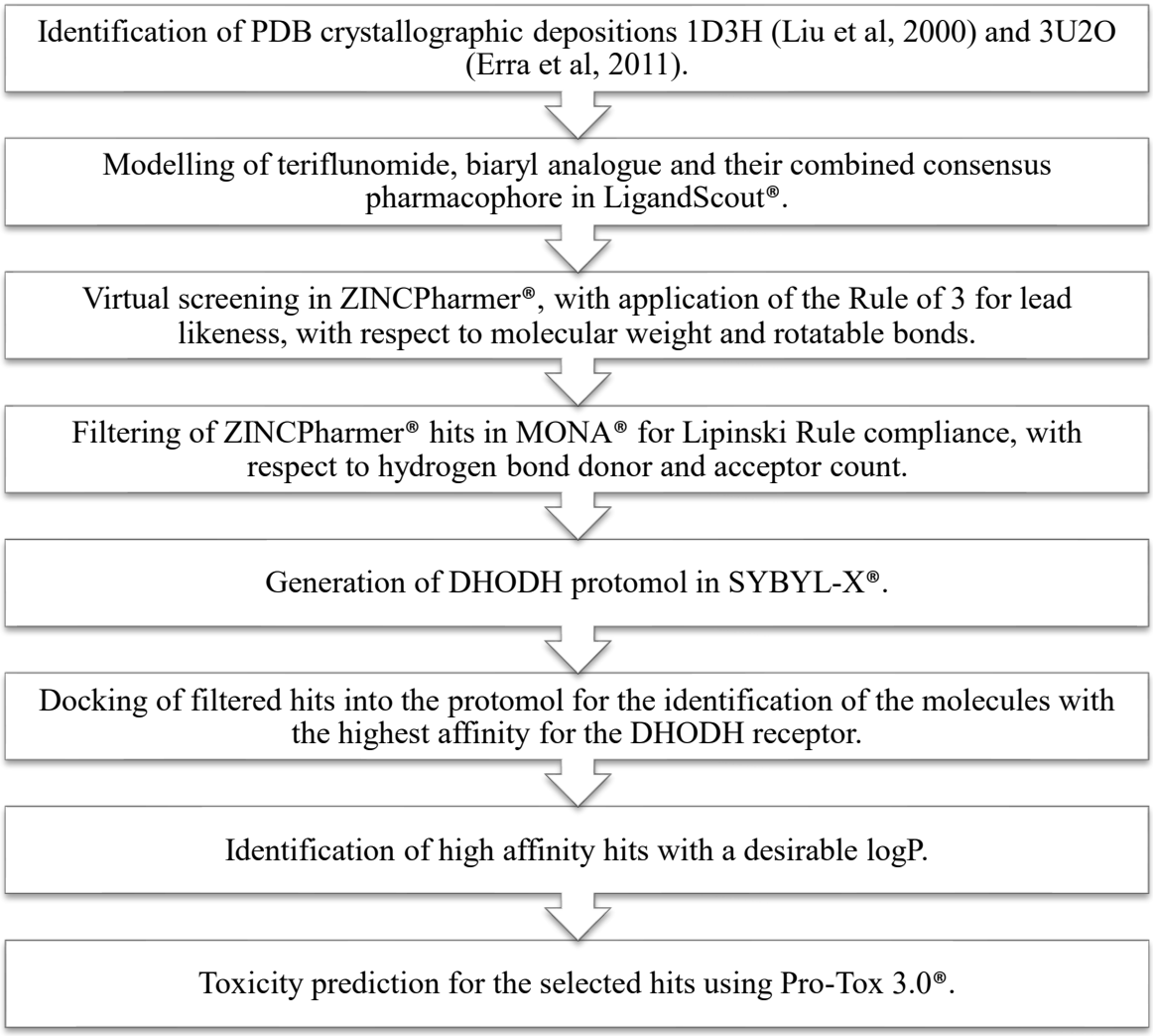

Figure 2.3 Flow Chart of the Virtual Screening Process.

2.3.2 Pharmacophore generation

Using PDB crystallographic deposition 1D3H (Liu *et al.*, 2000), a pharmacophore describing the critical contacts between teriflunomide and the DHODH receptor was created using LigandScout® (Wolber & Langer, 2005). A second pharmacophore describing the critical contacts between the biaryl analogue of teriflunomide and the DHODH receptor was created using PDB crystallographic deposition 3U2O (Erra *et al.*, 2011).

Using the teriflunomide and biaryl analogue pharmacophores, a consensus pharmacophore was generated in LigandScout® (Wolber & Langer, 2005), by placing them in the Alignment Perspective and selecting 'Generate Shared Feature Pharmacophore'. Teriflunomide was set as the reference molecule. The consensus pharmacophore was exported in pharmaceutical markup language (*.pml*) format.

Structure-based pharmacophores were generated since both the structure of the target (DHODH) and that of the ligand (teriflunomide or its biaryl analogue) were known. A consensus pharmacophore was then generated since the superimposition of pharmacophores to generate an average pharmacophore identifies the most important moieties in a compound required to elicit the desired response in a receptor and consequently, retrieve a cohort of molecules containing these moieties through virtual screening (Gaurav & Gautam, 2014).

2.3.3 Screening for Hit Molecules

The three pharmacophores were read into ZINCPharmer® (Koes & Camacho, 2012) for virtual screening with the application of the filters shown in Tables 2.1 and 2.2.

The filters selected in Table 2.1 aimed to decrease the number of hits for analysis since only the 2D properties of the hits were analysed after virtual screening, meaning that the different orientations and configurations of each molecule were not required. A low value for Root Mean Square Distance (RMSD) resulted in hits which have the best overall geometric match with the queried pharmacophore (Koes & Camacho, 2012).

Table 2.1 Hit Reduction Filters applied in ZINCPharmer® (Koes & Camacho, 2012).

Hit Reduction	
Maximum Hits per Configuration	1
Maximum Hits per Molecule	1
Maximum Total Hits	300
Maximum RMSD	1

The filters shown in Table 2.2 were imposed to obtain molecules which are lead-like. Lead-like molecules are easier to optimise since additional moieties can be added to the molecule without violating Lipinski's Rule of 5 (Lipinski *et al.*, 1996) for oral bioavailability. Some studies also suggest that a molecular weight below 300 Daltons decreases the risk of toxicity (Raymer & Bhattacharya, 2018).

Table 2.2 Hit Screening Filters applied in ZINCPharmer® (Koes & Camacho, 2012).

Hit Screening	
Molecular Weight	1-300 Daltons
Rotatable Bonds	1-3

The virtual screening process was carried out in the following databases:

- ZINC Purchasable: Last Updated 20/12/2014
- ZINC Purchasable Thiols: Last Updated 25/06/2013
- Alex Doemling UDC: Last Updated 26/02/2013
- ZINC Drug Database: Last Updated 23/09/2014
- ZINC In Man: Last Updated 23/09/2014
- ZINC Drug Database (Metabolites): Last Updated 22/09/2014
- ZINC Natural Derivatives: Last Updated 22/09/2014
- ZINC Natural Products: Last Updated 23/09/2014

The hits obtained were saved as *.sdf* files.

2.3.4 Filtering of Hits

The virtual screening hits obtained in ZINCPharmer® (Koes & Camacho, 2012) were filtered in MONA® (Hilbig & Rarey, 2015). Lipinski's Rule of 5 for oral bioavailability, with respect to hydrogen bond donor and acceptor count (Lipinski *et al.*, 1996), was used as the filtering criterion:

- Hydrogen bond acceptors: 1-10
- Hydrogen bond donors: 1-5

This process filtered the virtual screening hits in such a way that only drug-like and lead-like hits remained. Drug-like molecules are those which adhere to Lipinski's Rule of 5 for oral bioavailability (Lipinski *et al.*, 1996).

2.3.5 Protomol Generation

PDB crystallographic deposition 1D3H describing the bound coordinates of the DHODH receptor with antiproliferative agent A771726 (teriflunomide) (Liu *et al.*, 2000) was read into SYBYL-X® (Ash *et al.*, 2010). Water molecules and ions were removed and the protomol was generated using the Surflex Docking Mode, where the protomol generation mode was set to Ligand. The putative hits obtained in MONA® (Hilbig & Rarey, 2015) were docked into the protomol (using the Surflex Docking Mode) and a table of the affinities of the hits for the protomol, including their polar and crash scores, was created and saved as an *.xlsx* file.

A protomol is the energetically unsatisfied space in a receptor, thus a representation of the space occupied by an idealised ligand within the target receptor. As a result, the binding affinities of the hits to the protomol are an indication of the extent of occupation of the energetically unsatisfied space.

2.3.6 Identification of Hits with a desirable clogP

Using the Library View of LigandScout® (Wolber & Langer, 2005), the clogP values of teriflunomide and the molecules obtained from MONA® (Hilbig & Rarey, 2015) were determined. The molecules with a clogP higher than that of teriflunomide (clogP=2.140) were identified and ranked in order of affinity to the protomol. This exercise was performed in Microsoft Excel®.[5] The three molecules with the highest affinity for the protomol and a

[5] Microsoft. Excel®. Version 2508 [software]. Dassault Microsoft. 2024 [cited 2025 Jul 26; downloaded 2020 Oct 1]. Available from: https://excel.cloud.microsoft/en-gb/?wdOrigin=APPHOME-WEB.OTHER%2CAPPHOME-WEB.UNAUTH

clogP higher than 3 were selected, with the purpose of selecting of high affinity molecules with increased lipophilic characteristics.

2.3.7 Prediction of Toxicity for the Chosen Hits

The three molecules selected were read into Pro-Tox 3.0® (Banerjee *et al.*, 2024) using their Simplified Molecular Input Line Entry System (SMILES) notation to predict their median lethal dose (LD_{50}) and toxicity class when ingested orally. The SMILES notation for the molecules was obtained from the *.sdf* files read in BIOVIA® Draw.[3] A full toxicity report was generated for each molecule, and the immunotoxicity, hepatotoxicity and activity on the BBB were compared to those of teriflunomide, whose toxicity report was also generated for comparison. These toxicological endpoints were chosen to determine whether the molecules are likely to be immunosuppressive and hepatotoxic, the two being side-effects of the lead molecule teriflunomide (Biolato *et al.*, 2021).

[3] Dassault Systèmes. Biovia Draw®. Version 21.1 [software]. Dassault Systèmes. 2024 [cited 2025 Jul 26; downloaded 2023 Oct 19]. Available from: https://discover.3ds.com/biovia-draw-academic#_ga=2.9885366.2038323275.1652726867-4a55e360-cfd1-11ec-9db0-078235bac709.

2.4 De novo drug design

2.4.1 Overview of *de novo* drug design

Figure 2.4 shows a flow chart of the study design followed during the *de novo* drug design phase.

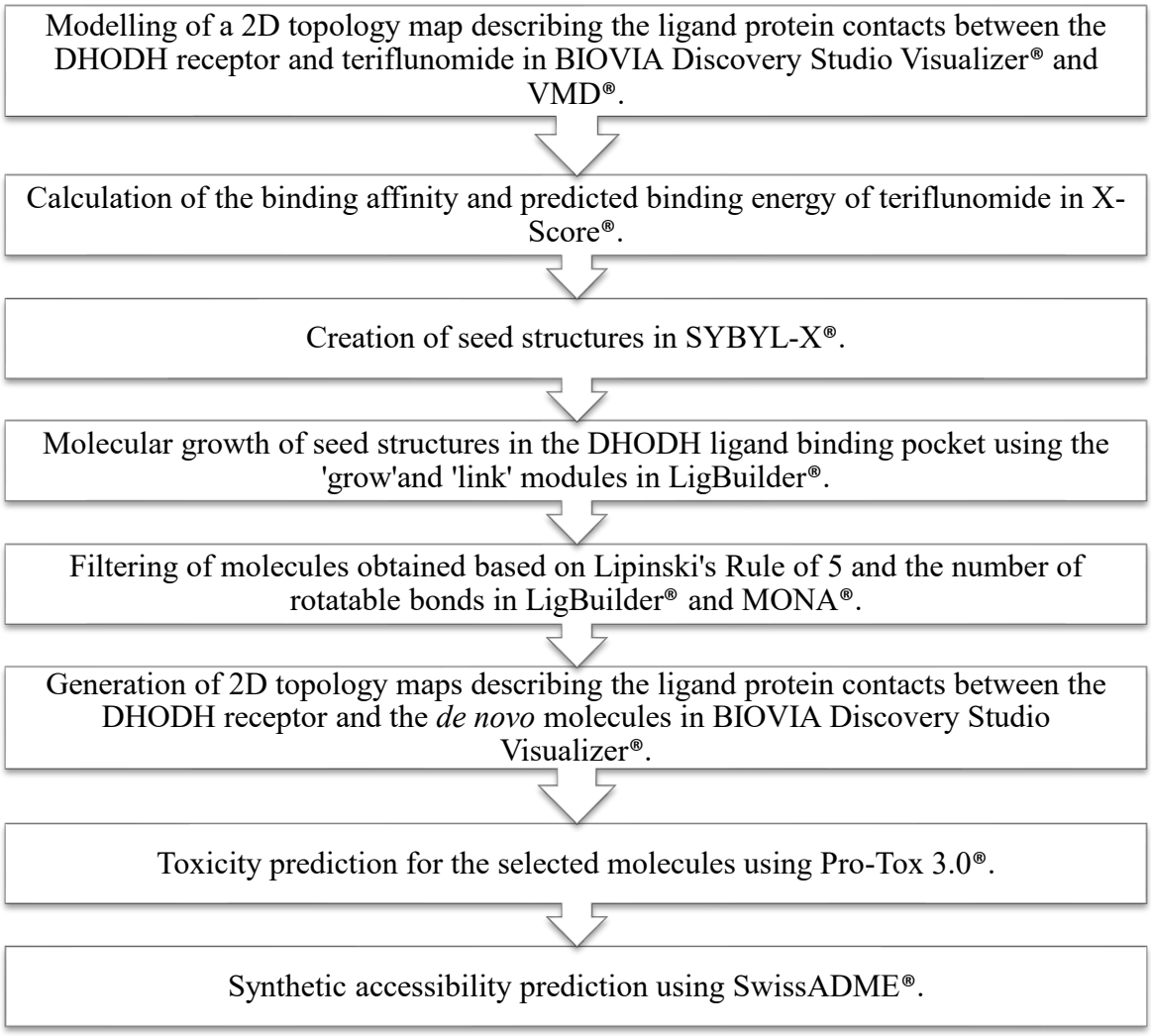

Figure 2.4 Flow Chart of the *de novo* Drug Design Process.

2.4.2 Receptor-Ligand Interactions Visualisation

PDB crystallographic deposition 1D3H (Liu *et al.*, 2000) was read into BIOVIA Discovery Studio Visualizer®.[4] In the 'Receptor-Ligands Interaction' tab, the receptor was defined as 1D3H and the ligand as A26397 (teriflunomide). 'Show 2D Diagram' was selected to generate a 2D topology map describing the ligand protein contacts between teriflunomide and the DHODH receptor. The purpose of the 2D topology map was to identify the moieties on teriflunomide which are responsible for its interactions with the ligand binding pocket of the DHODH receptor, as these give rise to the biological response.

2.4.3 DHODH Ligand Binding Pocket Determination

Using SYBYL-X® (Ash *et al.*, 2010) and PDB crystallographic deposition 1D3H (Liu *et al.*, 2000), the *apo* DHODH receptor was generated, by extracting the ligand teriflunomide into molecular space M2. The *apo* receptor was saved as a *.pdb* file and the extracted teriflunomide as a *.mol2* file.

A 3D model of the DHODH ligand binding pocket was generated using the 'pocket' module of LigBuilder® (Wang *et al.*, 2000), where the *apo* DHODH receptor and the extracted teriflunomide files generated in SYBYL-X® (Ash *et al.*, 2010) were used as the input files. The default parameter directory, minimal feature distance (3.5 Angstroms) and maximal feature number (8) within the preset *pocket.index* file were retained. These relatively low values for the minimal feature distance and the maximal feature number gave rise to a ligand binding pocket encompassing only its critical and distinct features. The DHODH ligand

[4]Dassault Systèmes. Biovia Discovery Studio Visualizer®. Version 24.1.0.23298 [software]. Dassault Systèmes. 2025 [cited 2025 Jul 25; downloaded 2024 Jan 16]. Available from: https://discover.3ds.com/discovery-studio-visualizer-download.

binding pocket, as circumscribed around the bioactive conformation of teriflunomide, was defined to later be used as the space within which seed structures were allowed to grow.

2.4.4 DHODH Ligand Binding Pocket Render

Rendering of teriflunomide within DHODH ligand binding pocket was carried out in VMD® (Humphrey *et al.*, 1996), by loading the key site file created in the 'pocket' module of LigBuilder® (Wang *et al.*, 2000) and the teriflunomide extract file created in SYBYL-X® (Ash *et al.*, 2010). The 3D DHODH ligand binding pocket model served as the space within which molecular growth from the seeds created in the next step was sustained. It is a mathematical calculation based on the interactions between teriflunomide and the DHODH receptor.

2.4.5 Binding Affinity Calculations for the Teriflunomide-DHODH receptor complex

The binding affinity and predicted binding energy of teriflunomide to the DHODH receptor were calculated in X-Score® (Wang *et al.*, 2002) using the *apo* receptor, and the extracted teriflunomide. Water molecules were removed, and all hydrogens were added to the *apo* receptor prior to initiating the exercise. No conformers of teriflunomide were generated for this step since the extracted teriflunomide (derived from PDB crystallographic deposition 1D3H (Liu *et al.*, 2000)) was already is in its bioactive conformation in the cognate DHODH receptor and since a low energy conformer is not necessarily bioactive (Habgood, 2017). The atomic binding score (pK_d) for each atom on the teriflunomide scaffold was calculated to determine which moieties on teriflunomide scaffold are mainly contributing towards the binding affinity.

2.4.6 Teriflunomide-based Seed Structure Generation

Seed structures based on the teriflunomide structure, differing in magnitude and growing site loci, were created in SYBYL-X® (Ash *et al.*, 2010), using the teriflunomide extract file created previously. It was ensured that all hydrogen atoms were added and that the valence of each atom in the structure was fulfilled to avoid the creation of chemically invalid structures (Wang *et al.*, 2000). Each structure was assigned one special hydrogen if earmarked for growth or two special hydrogens if earmarked for linking, when allowed to sustain growth within the DHODH ligand binding pocket. This process was guided by the 2D topology map and atomic binding scores generated in previous steps since these had identified the key moieties in the teriflunomide structure critical to binding.

2.4.7 Creation of Novel Molecules from Seed Structures

The seeds were allowed to grow at the predesignated special hydrogens within the DHODH ligand binding pocket using the 'grow' and 'link' modules of LigBuilder® (Wang *et al.*, 2000). The 'grow' module replaces the designated special hydrogens with fragments from the building block library, whereas the 'link' module also replaces the special hydrogens with fragments, but attempts to link them together to form a rational molecule (Yuan *et al.*, 2011). The default toxic and forbidden structures libraries within the *grow.index* and *link.index* files were used to exclude the creation of toxic and non-synthesisable structures. Figures 2.5 and 2.6 show the *grow.index* and *link.index* files used for this step.

```
#
# input files
#
SEED_LIGAND_FILE                        ../example/1d3h_grow.mol2
POCKET_ATOM_FILE                        ../example/1d3h_pocket.txt
POCKET_GRID_FILE                        ../example/1d3h_grid.txt
#
# force field directory
#
PARAMETER_DIRECTORY                     ../parameter/
#
# fragment libraries
#
BUILDING_BLOCK_LIBRARY                  ../fragment.mdb/
FORBIDDEN_STRUCTURE_LIBRARY             ../forbidden.mdb/
TOXIC_STRUCTURE_LIBRARY                 ../toxicity.mdb/
#
# structural construction parameters
#
GROWING_PROBABILITY                     1.00
LINKING_PROBABILITY                     0.50
MUTATION_PROBABILITY                    0.50
#
# chemical viability rules
#
APPLY_CHEMICAL_RULES                    YES
APPLY_FORBIDDEN_STRUCTURE_CHECK         YES
APPLY_TOXIC_STRUCTURE_CHECK             YES
MAXIMAL_MOLECULAR_WEIGHT                600
MINIMAL_MOLECULAR_WEIGHT                300
MAXIMAL_LOGP                            6.00
MINIMAL_LOGP                            3.00
MAXIMAL_HB_DONOR_ATOM                   6
MINIMAL_HB_DONOR_ATOM                   2
MAXIMAL_HB_ACCEPTOR_ATOM                6
MINIMAL_HB_ACCEPTOR_ATOM                2
MAXIMAL_PKD                             10.00
MINIMAL_PKD                             5.00
#
# genetic algorithm parameters
#
NUMBER_OF_GENERATION                    20
NUMBER_OF_POPULATION                    3000
NUMBER_OF_PARENTS                       200
ELITISM_RATIO                           0.10
SIMILARITY_CUTOFF                       0.90
#
# output files
#
POPULATION_RECORD_FILE                  population.lig
LIGAND_COLLECTION_FILE                  ligands.lig
#
```

Figure 2. 5 The *grow.index* file used to generate molecules, included for reproducibility purposes.

```
#
# input files
#
SEED_LIGAND_FILE                        ../example/1d3h_link.mol2
POCKET_ATOM_FILE                        ../example/1d3h_pocket.txt
POCKET_GRID_FILE                        ../example/1d3h_grid.txt
#
# force field directory
#
PARAMETER_DIRECTORY                     ../parameter/
#
# fragment libraries
#
BUILDING_BLOCK_LIBRARY                  ../fragment.mdb/
FORBIDDEN_STRUCTURE_LIBRARY             ../forbidden.mdb/
TOXIC_STRUCTURE_LIBRARY                 ../toxicity.mdb/
#
# structural building up parameters
#
GROWING_PROBABILITY                     1.00
LINKING_PROBABILITY                     1.00
MUTATION_PROBABILITY                    0.50
#
# chemical viability rules
#
APPLY_CHEMICAL_RULES                    YES
APPLY_FORBIDDEN_STRUCTURE_CHECK         YES
APPLY_TOXIC_STRUCTURE_CHECK             YES
MAXIMAL_MOLECULAR_WEIGHT                600
MINIMAL_MOLECULAR_WEIGHT                300
MAXIMAL_LOGP                            6.00
MINIMAL_LOGP                            3.00
MAXIMAL_HB_DONOR_ATOM                   6
MINIMAL_HB_DONOR_ATOM                   2
MAXIMAL_HB_ACCEPTOR_ATOM                6
MINIMAL_HB_ACCEPTOR_ATOM                2
MAXIMAL_PKD                             10.00
MINIMAL_PKD                             5.00
#
# genetic algorithm parameters
#
NUMBER_OF_GENERATION                    30000
NUMBER_OF_POPULATION                    1000
#
# output files
#
POPULATION_RECORD_FILE                  population.lig
LIGAND_COLLECTION_FILE                  ligands.lig
#
#
```

Figure 2.6 The *link.index* file used to generate molecules, included for reproducibility purposes.

2.4.8 Filtering of Molecules Generated

The output molecules were filtered using the 'process' module of LigBuilder® (Wang *et al.*, 2000). For this step, the *process.index* file shown in Figure 2.5 was used, with changes being made to the following criteria for molecules adherent to Lipinski's Rule of 5 (Lipinski *et al.*, 1996) and with an improved lipophilicity compared to teriflunomide to be selected:

- Molecular weight: 300-500 Da
- LogP: 3-5

```
#
# input files
#
LIGAND_COLLECTION_FILE                  ligands.lig
#
# chemical rules
#
MAXIMAL_MOLECULAR_WEIGHT                600
MINIMAL_MOLECULAR_WEIGHT                300
MAXIMAL_LOGP                            6.00
MINIMAL_LOGP                            3.00
MAXIMAL_PKD                             10.00
MINIMAL_PKD                             5.00
#
# similarity threshhold
#
SIMILARITY_CUTOFF                       0.90
#
# output files
#
NUMBER_OF_OUTPUT_MOLECULES              200
OUTPUT_DIRECTORY                        results.mdb/
#
```

Figure 2.7 The process.index file used to generate molecules, included for reproducibility purposes.

The filtered molecules were then filtered in MONA® (Hilbig & Rarey, 2015) using the following criteria:

- Hydrogen bond acceptor count: 1-10
- Hydrogen bond donor count: 1-5
- Number of rotatable bonds: 1-3

The filtering criteria resulted in molecules which have drug-like properties.

2.4.9 Generation of 2D topology maps for the *de novo* molecules

For each of the *de novo* molecule, a 2D topology map describing their contacts with the DHODH receptor was generated in BIOVIA Discovery Studio Visualizer®.[4] The *apo* DHODH receptor and the selected molecule were uploaded and defined as the receptor and ligand, respectively, in the 'Receptor-Ligand Interactions' tab. 'Show 2D diagram' generated the 2D topology maps.

2.4.10 Renders of the *de novo* molecules within the DHODH ligand binding pocket

Rendering of the *de novo* molecules within DHODH ligand binding pocket was carried out in VMD (Humphrey *et al.*, 1996), following the same procedure used for the render of teriflunomide within the DHODH ligand binding pocket.

2.4.11 Prediction of Toxicity for the *de novo* Molecules

Using the SMILES notation, the molecules were read into Pro-Tox 3.0® (Banerjee *et al.*, 2024) to predict their LD_{50} and toxicity class when ingested orally. A full toxicity report was generated for each molecule, and the immunotoxicity, hepatotoxicity and activity on the BBB were compared to those of teriflunomide.

[4] Dassault Systèmes. Biovia Discovery Studio Visualizer®. Version 24.1.0.23298 [software]. Dassault Systèmes. 2025 [cited 2025 Jul 25; downloaded 2024 Jan 16]. Available from: https://discover.3ds.com/discovery-studio-visualizer-download.

2.4.12 Prediction of Synthetic Accessibility for the *de novo* Molecules

The molecules were uploaded to SwissADME® (Daina *et al.*, 2017) to determine their synthetic accessibility since it is unknown whether synthetic routes for these molecules exist and whether they are feasible or not.

2.5 Submission to Faculty Research Ethics Committee

A research proposal (Appendix 1-Application ID MED-2024-00121) was submitted for filing purposes to the Faculty of Medicine and Surgery Research Ethics Committee.

Chapter 3

Results

3.1 Virtual Screening

3.1.1 Pharmacophores

Table 3.1 defines the pharmacophoric features observed in the pharmacophores generated in LigandScout®(Wolber & Langer, 2005).

Table 3.1 Pharmacophore Feature Definitions.

Depiction in LigandScout®	**Pharmacophore feature**
	Hydrophobic Interactions
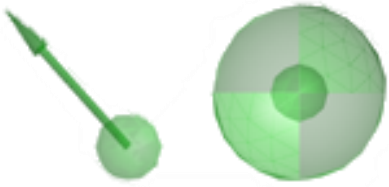	Hydrogen Bond Donor
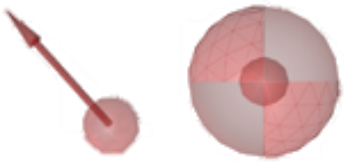	Hydrogen Bond Acceptor

The teriflunomide pharmacophore generated in LigandScout® (Wolber & Langer, 2005) is shown in Figure 3.1. It consists of three regions of hydrophobic interactions (benzene ring, methyl group and trifluoromethyl group), one hydrogen bond donor (hydroxyl group) and three hydrogen bond acceptors (carbonyl group, hydroxyl group and nitrile group).

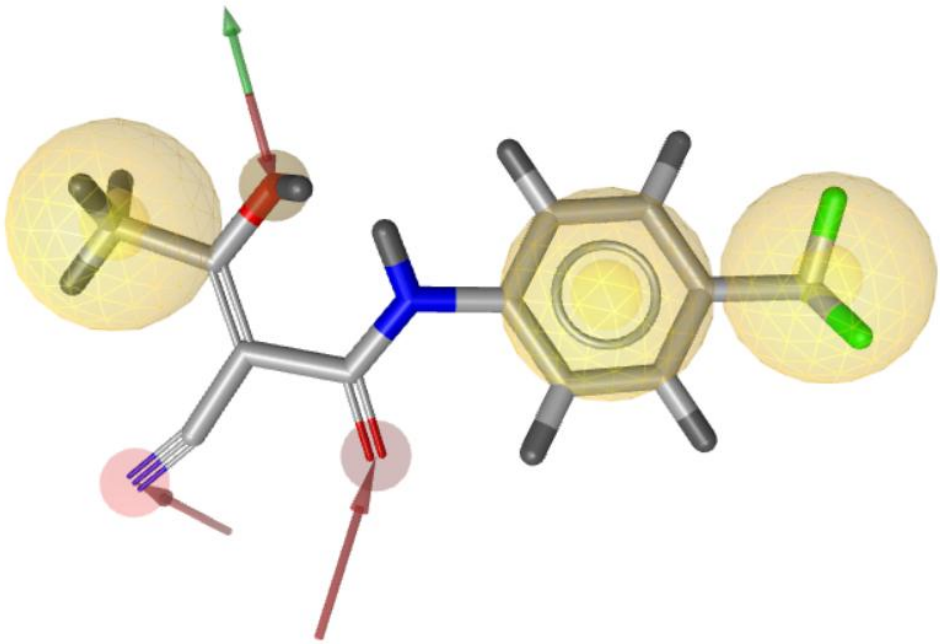

Figure 3.1 The bioactive conformation of teriflunomide as described in PDB crystallographic deposition 1D3H (Liu *et al*., 2000) superimposed onto its pharmacophore, as rendered in LigandScout® (Wolber & Langer, 2005).

Figure 3.2 shows the critical interactions forged between teriflunomide and the DHODH ligand binding pocket.

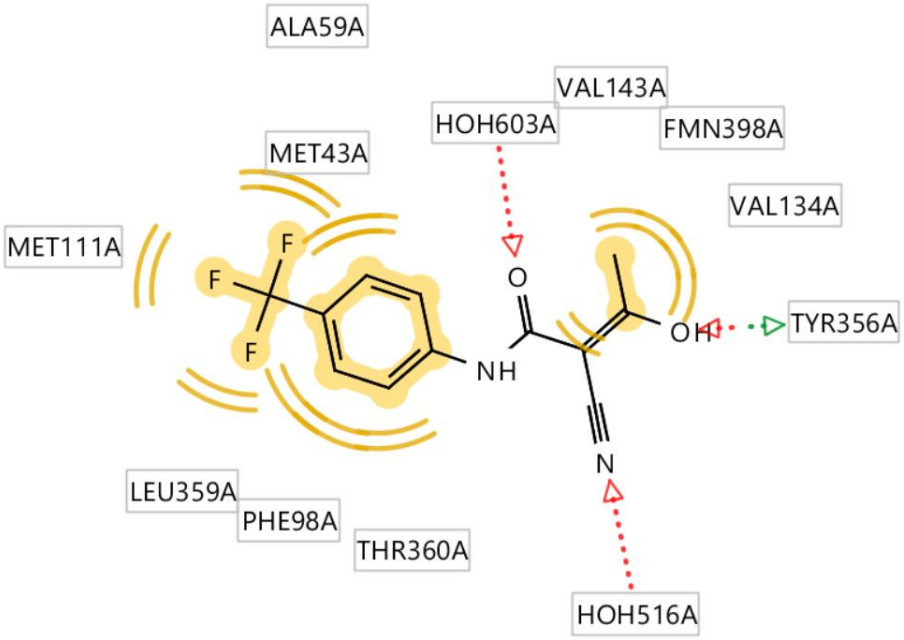

Figure 3.2 The 2D bioactive conformation of teriflunomide showing the critical points of contact formed between teriflunomide and the amino acids lining the ligand binding pocket of DHODH, as rendered in LigandScout® (Wolber & Langer, 2005).

Figure 3.3 shows the pharmacophore generated for the biaryl analogue of teriflunomide. It consists of four regions of hydrophobic interactions (two benzene rings, ethyl group and fluorine atom) one hydrogen bond donor (hydroxyl group) and three hydrogen bond acceptors (carbonyl group, hydroxyl group and nitrile group).

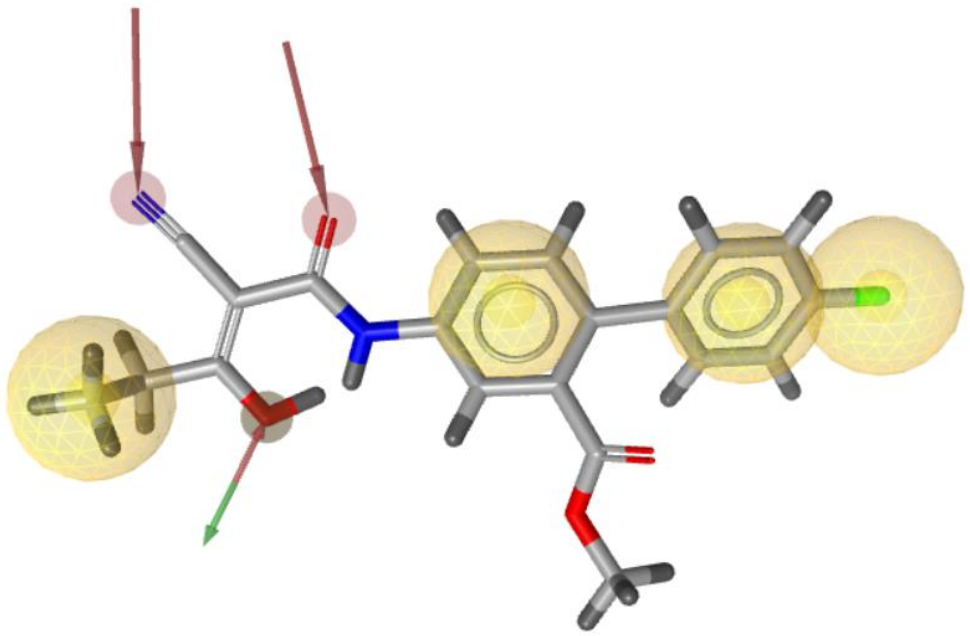

Figure 3. 3 The bioactive conformation of the small molecule inhibitor as described in PDB crystallographic deposition 3U2O (Erra *et al.*, 2011) superimposed onto its pharmacophore, as rendered in LigandScout® (Wolber & Langer, 2005).

Figure 3.4 shows the critical interactions between the biaryl analogue of teriflunomide and the DHODH ligand binding pocket.

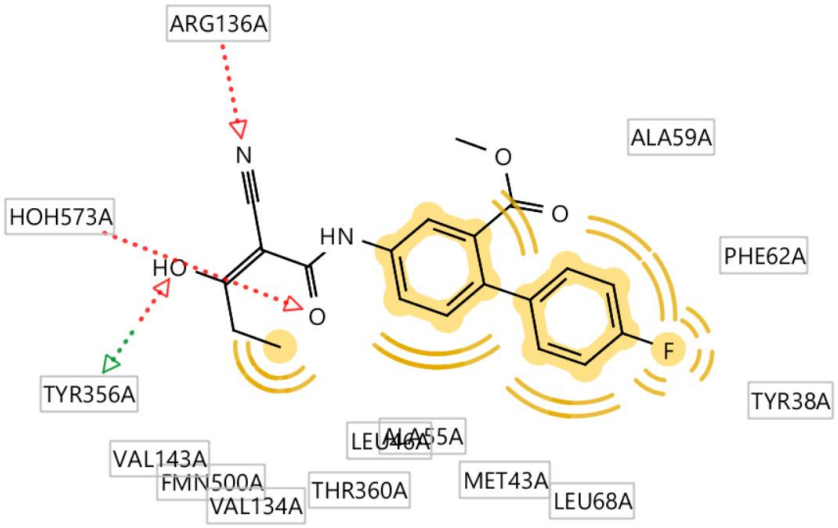

Figure 3.4 The 2D bioactive conformation of the biaryl analogue of teriflunomide showing the critical points of contact formed between the biaryl analogue and the amino acids lining the ligand binding pocket of DHODH, as rendered in LigandScout® (Wolber & Langer, 2005).

Figure 3.5 shows the consensus pharmacophore of teriflunomide and its biaryl analogue. It consists of two areas of hydrophobic interactions, three hydrogen bond acceptors and one hydrogen bond donor.

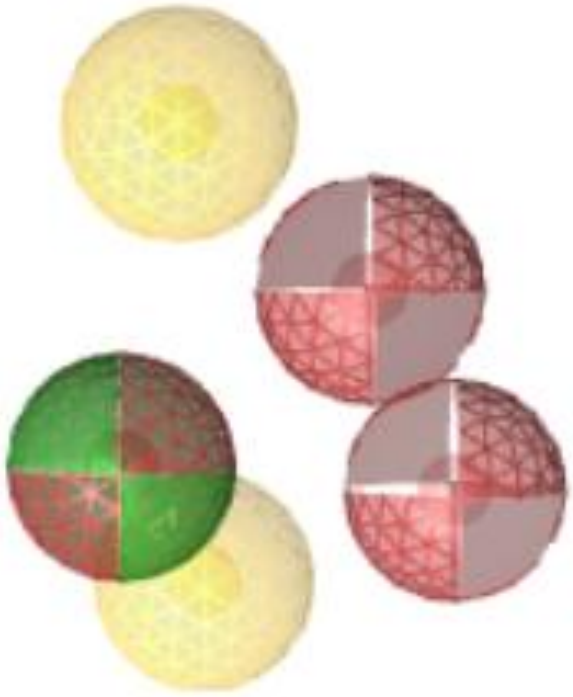

Figure 3.5 The consensus pharmacophore of teriflunomide and the small molecule inhibitor, rendered in LigandScout® (Wolber & Langer, 2005).

3.1.2 ZINCPharmer® Results

The results obtained through virtual screening in ZINCPharmer® (Koes & Camacho, 2012), are shown in Table 3.2.

Table 3.2 Number of hits obtained in ZINCPharmer® (Koes & Camacho, 2012) for the consensus pharmacophore.

Database	**Number of Hits obtained for the Consensus Pharmacophore**
ZINC Purchasable	300
ZINC Natural Products	34
ZINC Purchasable Thiols	15
ZINC Natural Derivatives	14
Alex Doemling UDC	11
ZINC In Man	1
ZINC Drug Database	0
ZINC Drug Database (Metabolites)	0

No hits were obtained for the pharmacophore of the biaryl analogue of teriflunomide. Three hits were obtained for the pharmacophore of teriflunomide in the ZINC Purchasable database. Eliminating duplicate hits resulted in a total of 353 hits, of which 299 hits were determined to be Lipinski Rule of 5 compliant (Lipinski *et al.*, 1996).

3.1.3 DHODH protomol

Figure 3.6 shows the protomol created in SYBYL-X® (Ash *et al.*, 2010).

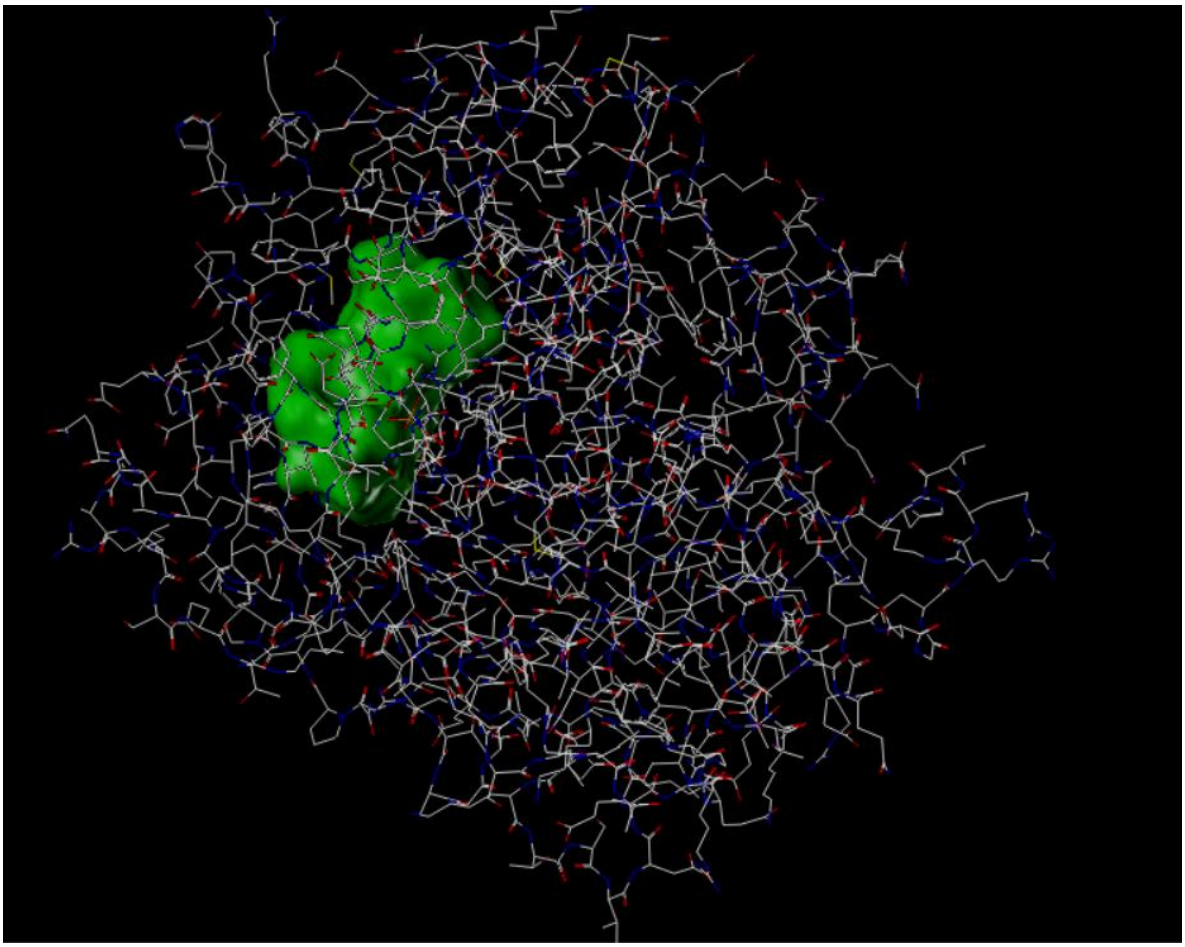

Figure 3.6 The protomol describing the energetically unsatisfied space within the DHODH receptor as described in PDB crystallographic deposition 1D3H, describing the bound coordinates of the DHODH receptor with teriflunomide (Liu *et al.*, 2000), generated in SYBYL-X® (Ash *et al.*, 2010).

3.1.4 Structures and Properties of the Selected Hits

Table 3.3 shows the 3D and 2D structures of the three hits having the highest affinity for the protomol and a desirable clogP (>2.14=clogP of teriflunomide (Liu *et al.*, 2000)). The three hits selected are all based on the consensus pharmacophore and originated from the ZINC Purchasable database.

Table 3.3 3D and 2D structures of the selected hits, rendered in BIOVIA Discovery Studio Visualizer® and BIOVIA Draw®, respectively.[3, 4]

Name of molecule	3D structure of molecule	2D structure of molecule
ZINC73182521	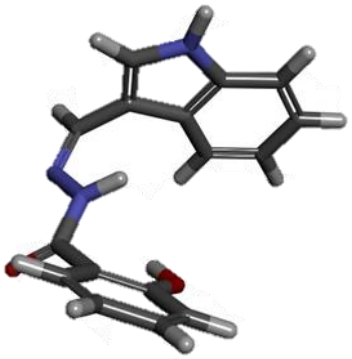	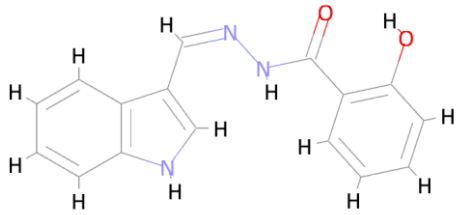
ZINC06536819	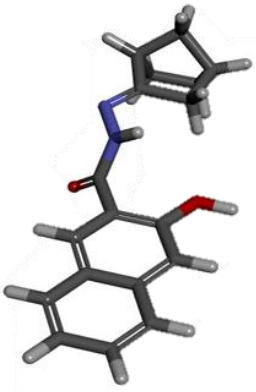	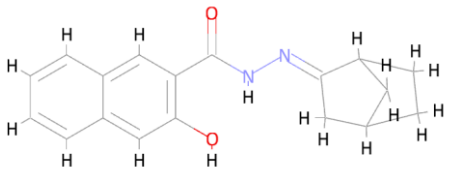
ZINC81626129	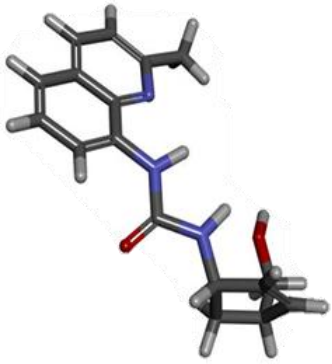	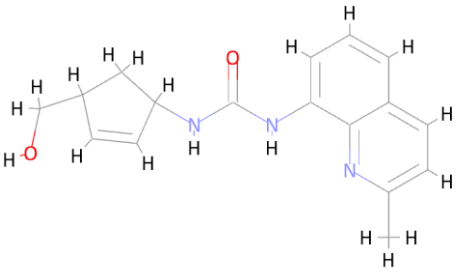

[3] Dassault Systèmes. Biovia Draw®. Version 21.1 [software]. Dassault Systèmes. 2024 [cited 2025 Jul 26; downloaded 2023 Oct 19]. Available from: https://discover.3ds.com/biovia-draw-academic#_ga=2.9885366.2038323275.1652726867-4a55e360-cfd1-11ec-9db0-078235bac709.

Table 3.4 shows the affinity for the protomol, the polar and crash scores and the clogP of the selected hits.

Table 3.4 Total Score, Polar Score, Crash Score and clogP of the selected hits.

Name of molecule	**Affinity for the protomol (Total Score)**	**Polar Score**	**Crash Score**	**clogP**
ZINC73182521	4.9	2.56	-0.56	2.64
ZINC06536819	4.83	1.72	-1.06	3.45
ZINC81626129	4.7	1.66	-0.68	2.60

[4] Dassault Systèmes. Biovia Discovery Studio Visualizer®. Version 24.1.0.23298 [software]. Dassault Systèmes. 2025 [cited 2025 Jul 25; downloaded 2024 Jan 16]. Available from: https://discover.3ds.com/discovery-studio-visualizer-download.

Table 3.5 shows the properties of the molecules chosen, which predispose them to oral bioavailability, as calculated by LigandScout® (Wolber & Langer, 2005).

Table 3.5 The properties of the selected molecules which predispose them to oral bioavailability.

Name of molecule	**Molecular Weight (Da)**	**Number of hydrogen bond donors**	**Number of hydrogen bond acceptors**	**Number of simple rotatable bonds**
ZINC73182521	279.30	3	3	3
ZINC06536819	294.35	2	3	2
ZINC81626129	297.36	3	3	3

Table 3.6 shows an extract of the toxicological properties from the toxicity reports generated by Pro-Tox 3.0® (Banerjee *et al.*, 2018), compared to those of teriflunomide.

Table 3.6 The toxicity endpoints of teriflunomide and the virtual screening hit molecules selected.

Molecule	**Predicted LD_{50} (mg/kg)**	**Toxicity Class**	**Hepatotoxicity**	**Immunotoxicity**	**BBB Activity**
Teriflunomide	160	3	Active	Inactive	Inactive
ZINC73182521	375	4	Active	Inactive	Active
ZINC06536819	324	4	Inactive	Inactive	Active
ZINC81626129	2000	4	Inactive	Active	Active

Toxicity class 3 indicates that the molecule is toxic when swallowed whereas toxicity class 4 indicates that the molecule is harmful if swallowed.

3.2 *De novo* Drug Design

3.2.1 Receptor-Ligand Interactions Visualisation

Figure 3.7 shows the 2D topology map depicting the critical interactions between teriflunomide and the DHODH receptor in BIOVIA Discovery Studio Visualizer®.[4]

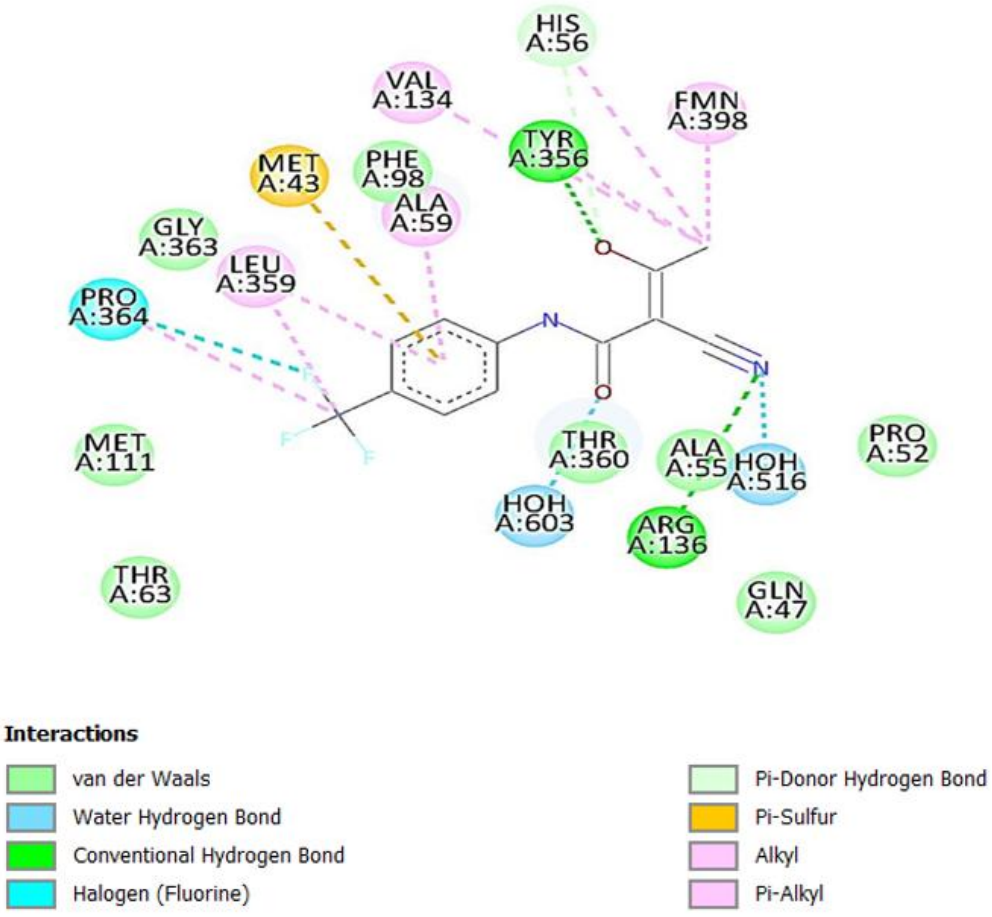

Figure 3.7 2D topology map showing the critical interactions forged between teriflunomide and the DHODH receptor, rendered in BIOVIA Discovery Studio Visualizer®.[4]

[4] Dassault Systèmes. Biovia Discovery Studio Visualizer®. Version 24.1.0.23298 [software]. Dassault Systèmes. 2025 [cited 2025 Jul 25; downloaded 2024 Jan 16]. Available from: https://discover.3ds.com/discovery-studio-visualizer-download.

3.2.2 DHODH Ligand Binding Pocket Render

Figure 3.8 shows a 3D representation created in VMD® (Humphrey *et al.*, 1996) of the DHODH ligand binding pocket, superimposed on the structure of teriflunomide.

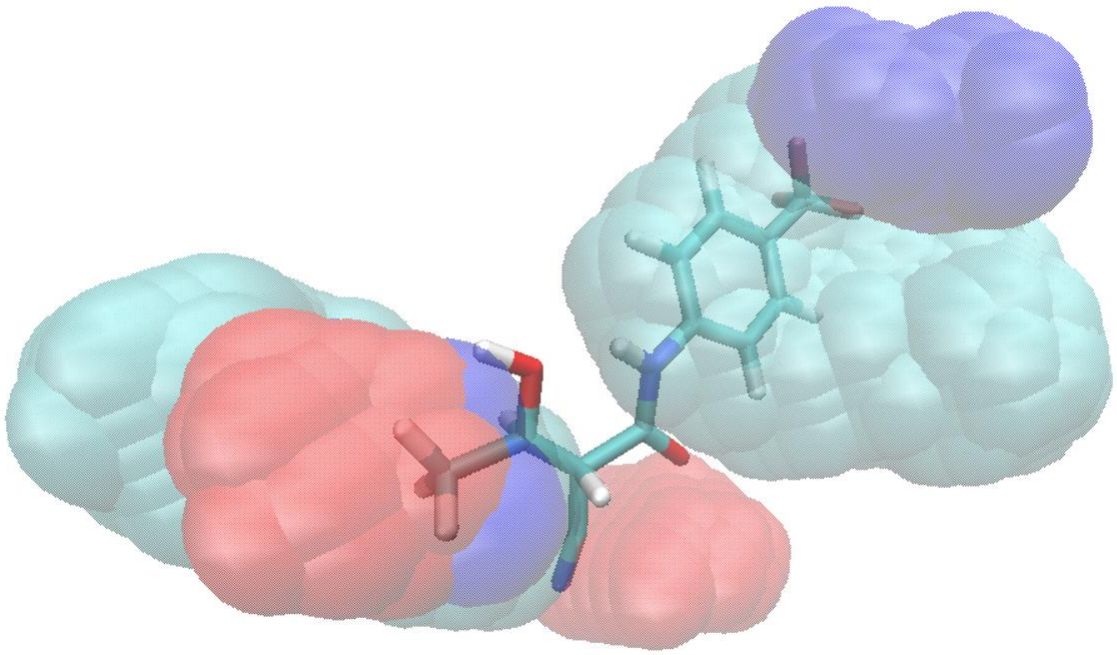

Figure 3.8 A 3D visualisation of teriflunomide within the DHODH ligand binding pocket, rendered in VMD® (Humphrey *et al.*, 1996). The hydrophobic areas are depicted in green, the hydrogen bond donors in blue and the hydrogen bond acceptors in red.

3.2.3 Binding Affinity Calculations

Table 3.7 shows the binding affinity and predicted binding energy of teriflunomide to the DHODH receptor, calculated in X-Score® (Wang *et al.*, 2002).

Table 3.7 Binding affinity and predicted binding energy of teriflunomide to the DHODH receptor.

Parameter	**Value**
Binding affinity (pK_d)	5.99
Predicted binding energy ($kcalmol^{-1}$)	-8.28

Figure 3.9 shows the Atom ID assigned to each atom on the teriflunomide scaffold. The hydrogen atoms were not included since they did not contribute to the binding affinity of the molecule.

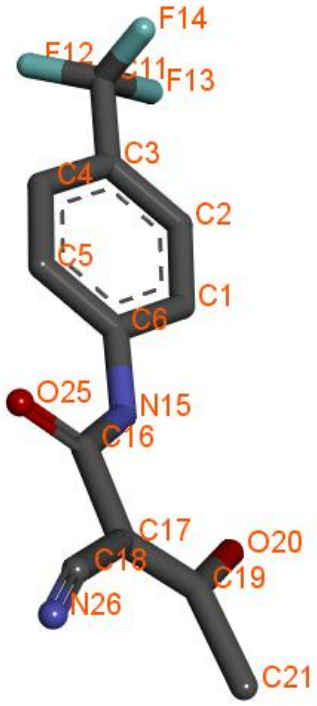

Figure 3.9 Structure of teriflunomide with Atom IDs, rendered in BIOVIA Discovery Studio Visualizer®.[4]

[4] Dassault Systèmes. Biovia Discovery Studio Visualizer®. Version 24.1.0.23298 [software]. Dassault Systèmes. 2025 [cited 2025 Jul 25; downloaded 2024 Jan 16]. Available from: https://discover.3ds.com/discovery-studio-visualizer-download.

Table 3.8 shows the atom binding score for each atom (excluding hydrogens) present on teriflunomide, as calculated by X-Score® (Wang *et al.*, 2002).

Table 3.8 Atom Binding Score for the atoms present on the teriflunomide scaffold.

Atom ID	**Atom Binding Score (pK_d)**
N26	0.29
C18	0.26
C17	0.29
C19	0.27
C21	0.52
O20	0.36
C16	0.25
O25	0.27
N15	0.28
C6	0.30
C5	0.37
C4	0.37
C3	0.32
C11	0.26
F14	0.27
F13	0.26
F12	0.25
C2	0.40
C1	0.41

3.2.4 Structures and Properties of the Molecules Generated

For this step, a total of 35 seeds were created in SYBYL-X® (Ash *et al.*, 2010). From the seeds created for molecular growth using the 'grow' module of LigBuilder® (Wang *et al.*, 2000), four of them generated a total of 32,144 molecules, of which 24,609 molecules met the criteria set for filtering using the process module of LigBuilder® (Wang *et al.*, 2000). Filtering in MONA® (Hilbig & Rarey, 2015) for Lipinski Rule (Lipinski *et al.*, 1996) compliance resulted in six molecules, derived from three seed structures. None of the seed structures created for molecular growth using the 'link' module of LigBuilder® (Wang *et al.*, 2000) generated any molecules.

Table 3.9 shows the 3D and 2D structures of the seed molecules created, which produced molecules compliant with the pre-established inclusion criteria, when subjected to growth within the DHODH ligand binding pocket.

Table 3.9 3D and 2D structures of the seed molecules created, rendered in BIOVIA Discovery Studio Visualizer® and BIOVIA Draw®, respectively.[3, 4] The hydrogen atoms circled in red are the special hydrogen atoms on which molecular growth was allowed to occur.

Seed ID	**3D structure**	**2D structure**
Seed 30		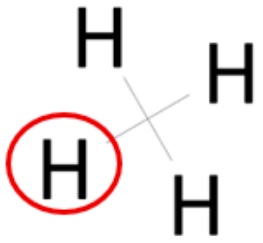
Seed 33	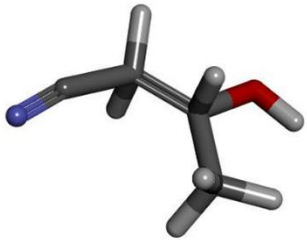	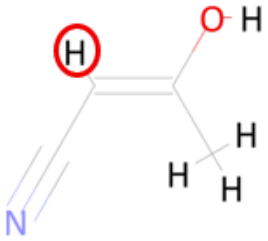
Seed 34	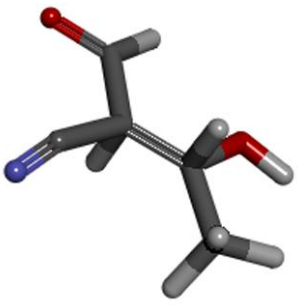	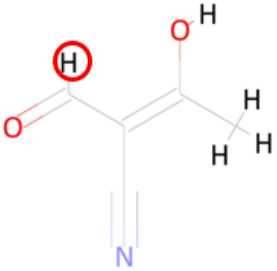

Table 3.10 shows the 3D and 2D structures of the molecules generated, which are compliant the pre-established inclusion criteria.

Table 3.10 3D and 2D structures of the *de novo* molecules compliant with the pre-established inclusion criteria, rendered in LigandScout® (Wolber & Langer, 2005) and BIOVIA Draw®[3], respectively.

Molecule ID	**Structure of molecule**
Seed30_Result195	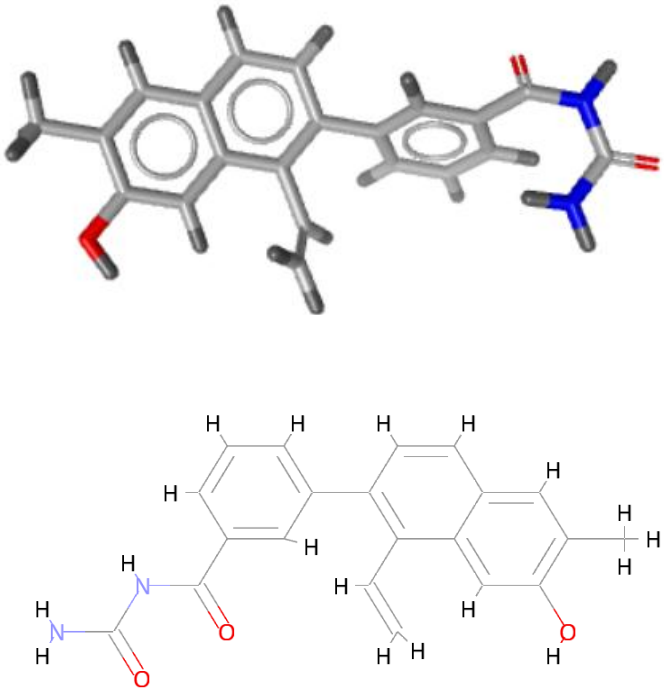

[3] Dassault Systèmes. Biovia Draw®. Version 21.1 [software]. Dassault Systèmes. 2024 [cited 2025 Jul 26; downloaded 2023 Oct 19]. Available from: https://discover.3ds.com/biovia-draw-academic#_ga=2.9885366.2038323275.1652726867-4a55e360-cfd1-11ec-9db0-078235bac709.

Seed30_Result196	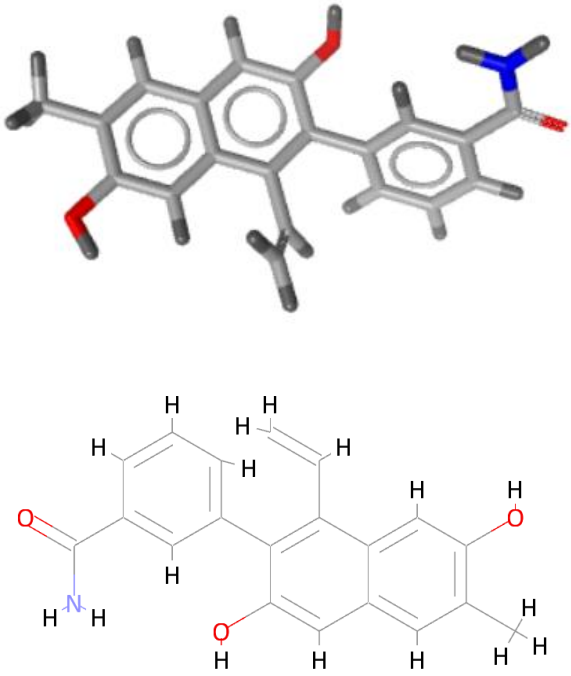
Seed33_Result099	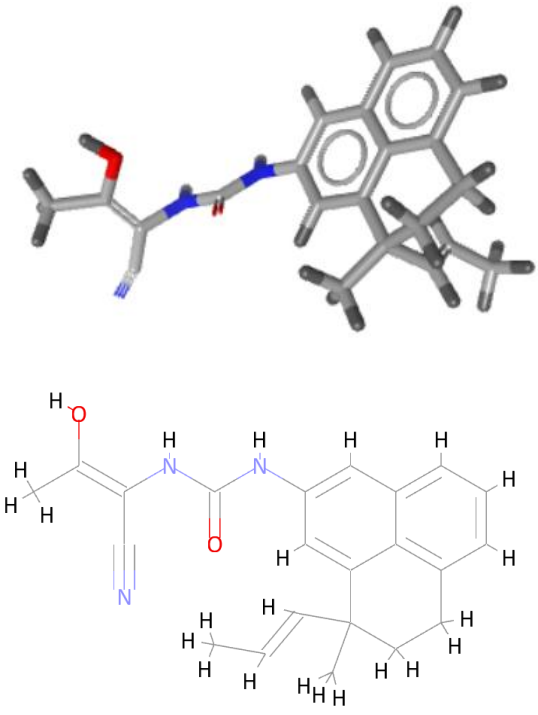

Seed33_Result103	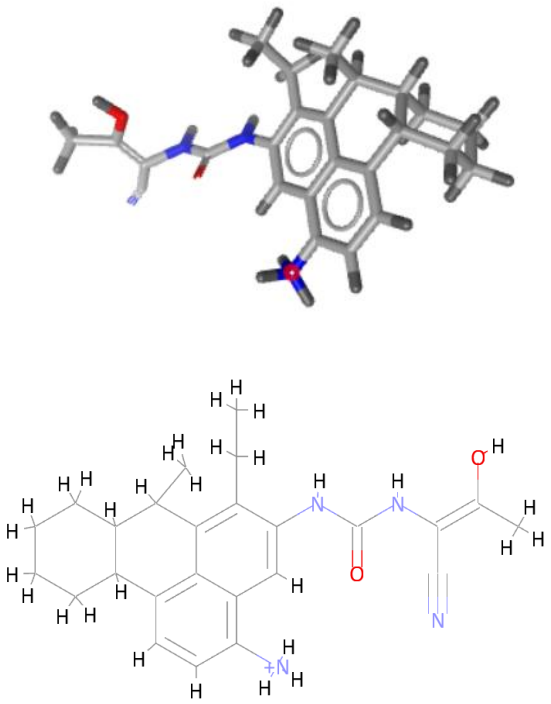
Seed33_Result199	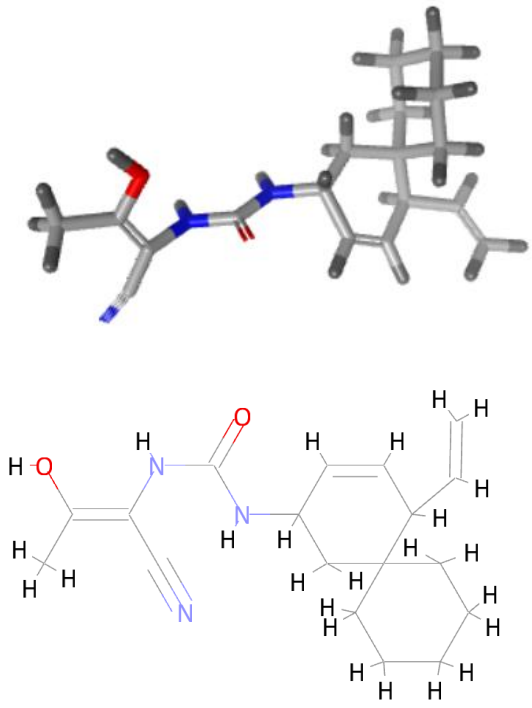

Seed34_Result194	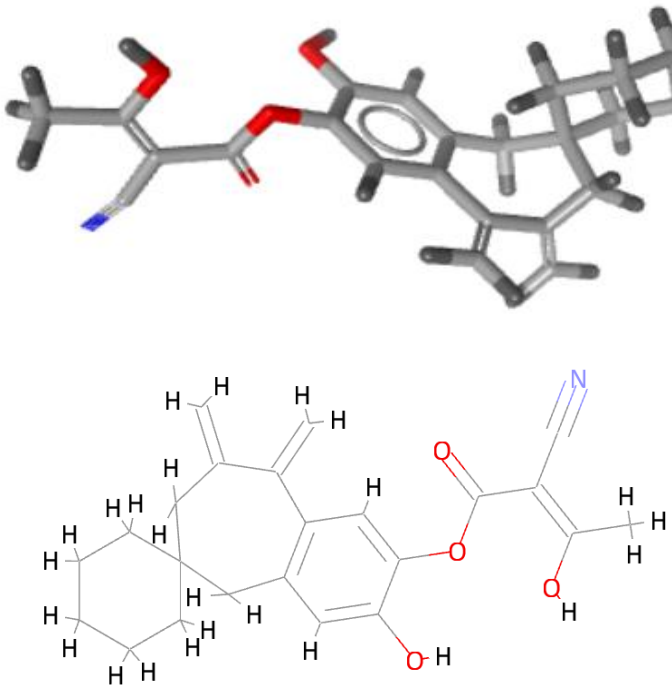

Table 3.11 shows the binding score and the clogP of the molecules generated, as calculated by the 'grow' module of LigBuilder® (Wang *et al.*, 2000).

Table 3.11 Binding score and clogP of the generated molecules.

Molecule ID	**Binding score (pKd)**	**clogP**
Seed30_Result195	8.45	4.96
Seed30_Result196	8.27	4.47
Seed33_Result099	7.74	4.68
Seed33_Result103	7.72	4.61
Seed33_Result199	7.68	3.57
Seed34_Result194	8.75	4.50

Table 3.12 shows the properties of the molecules chosen, which predispose them to oral bioavailability, as calculated by LigandScout® (Wolber & Langer, 2005).

Table 3.12 Select properties of the resultant *de novo* molecules.

Molecule ID	**Molecular weight (Da)**	**Number of hydrogen bond donors**	**Number of hydrogen bond acceptors**	**Number of simple rotatable bonds**
Seed30_Result195	346.38	3	3	3
Seed30_Result196	319.36	3	3	3
Seed33_Result099	361.44	3	3	3
Seed33_Result103	419.55	4	3	3
Seed33_Result199	315.41	3	3	3
Seed34_Result194	379.45	2	5	3

Table 3.13 shows an extract of toxicological reports generated in Pro-Tox 3.0® (Banerjee *et al.*, 2018).

Table 3.13 The toxicity endpoints of *de novo* molecules.

Molecule ID	**Predicted LD_{50} (mg/kg)**	**Toxicity Class**	**Hepato-toxicity**	**Immuno-toxicity**	**BBB Activity**
Seed30_Result195	200	3	Active	Active	Active
Seed30_Result196	200	3	Active	Active	Active
Seed33_Result099	200	3	Active	Inactive	Active
Seed33_Result103	200	3	Inactive	Inactive	Active
Seed33_Result199	9500	6	Inactive	Inactive	Active
Seed33_Result194	2000	4	Inactive	Inactive	Active

Toxicity class 3 indicates that the molecule is toxic when swallowed whereas toxicity class 4 indicates that the molecule is harmful if swallowed. A molecule with toxicity class 6 is non-toxic.

Table 3.14 shows the synthetic accessibility score of the molecules, as calculated in SwissADME® (Daina *et al.*, 2017). Synthetic accessibility is rated on a scale from 1-10, where a score of 1 indicates that the molecule is very easy to synthesise and a score of 10 indicates that the molecule is very difficult to synthesise.

Table 3.14 The synthetic accessibility score of the *de novo* molecules.

Molecule	**Synthetic accessibility score**
Seed30_Result195	2.58
Seed30_Result196	2.58
Seed33_Result099	4.02
Seed33_Result103	Molecule too large for calculation.
Seed33_Result199	5.04
Seed34_Result194	4.11

3.2.5 2D Topology Maps and Renders for the Generated Molecules

Table 3.15 shows 2D topology maps depicting the critical interactions between the *de novo* molecules and the DHODH receptor in BIOVIA Discovery Studio Visualizer®[4] and 3D representations of the DHODH ligand binding pocket, superimposed on the structures of the *de novo* molecules, created in VMD® (Humphrey *et al.*, 1996).

[4] Dassault Systèmes. Biovia Discovery Studio Visualizer®. Version 24.1.0.23298 [software]. Dassault Systèmes. 2025 [cited 2025 Jul 25; downloaded 2024 Jan 16]. Available from: https://discover.3ds.com/discovery-studio-visualizer-download.

Table 3.15 The 2D topology maps and 3D representations within the DHODH ligand binding pocket of the *de novo* molecules, rendered in BIOVIA Discovery Studio Visualizer®[4] and VMD® (Humphrey *et al.*, 1996), respectively.

Molecule ID	**Molecules within the DHODH Ligand Binding Pocket.**
Seed30_Result195	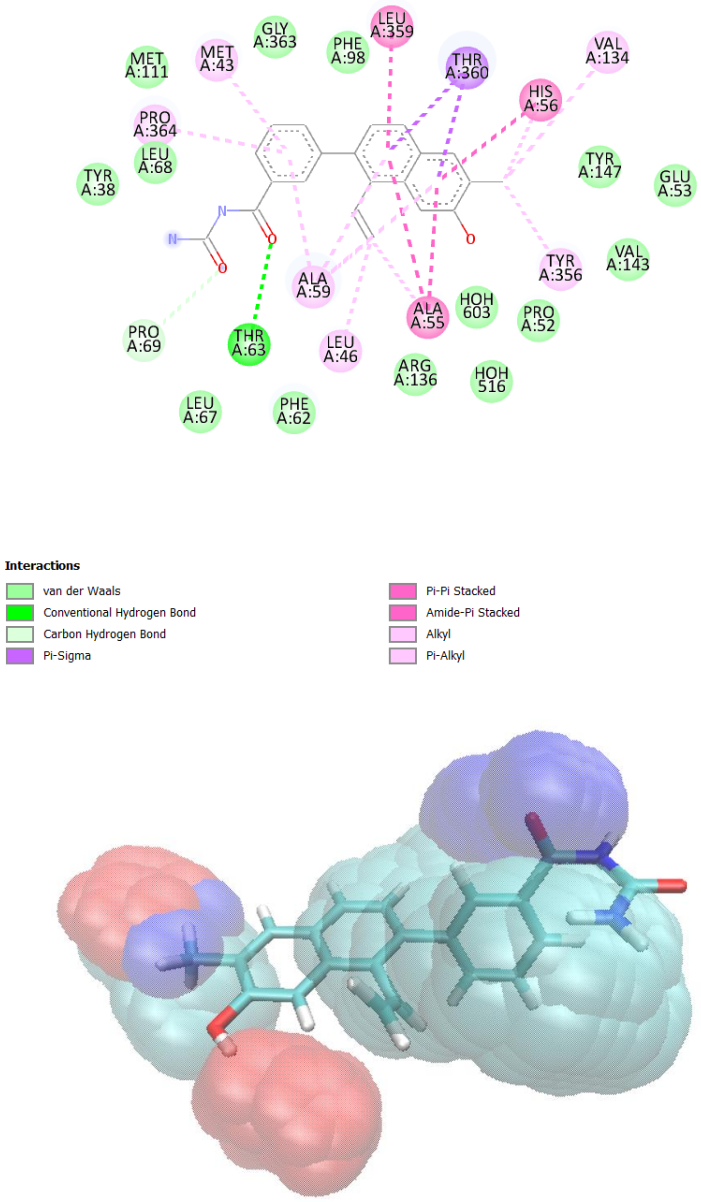

Seed30_Result196	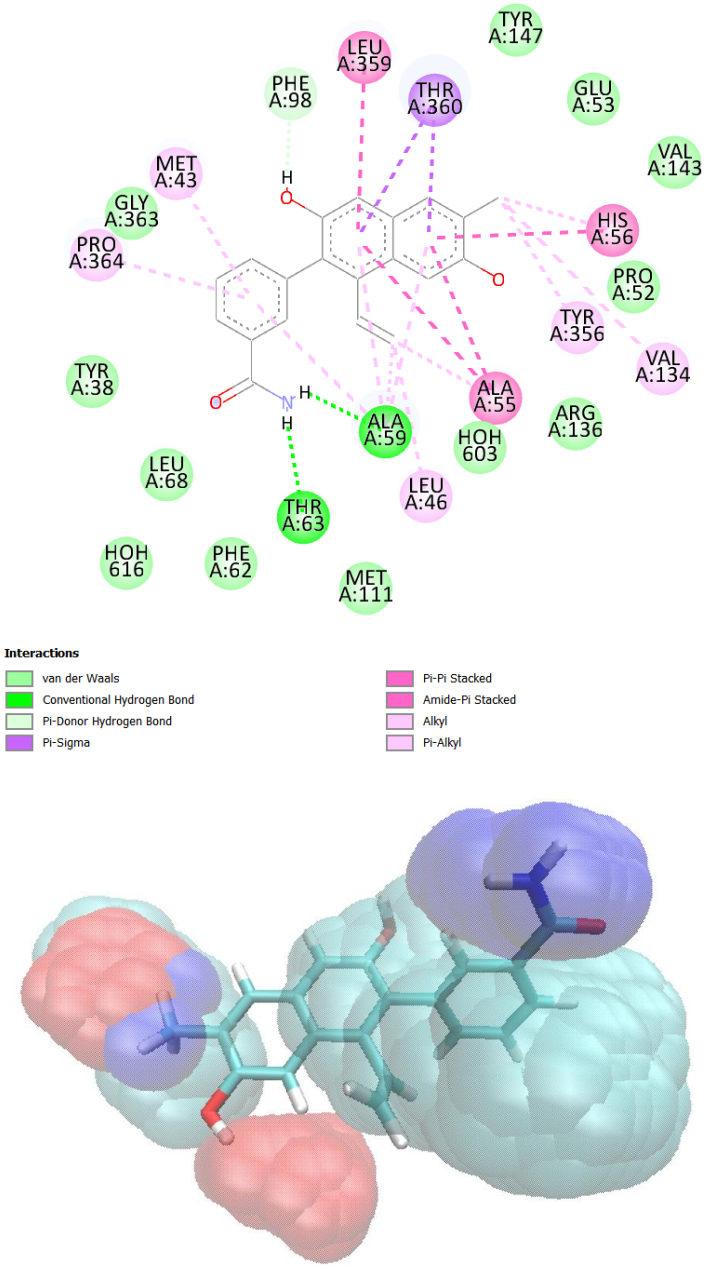

Seed33_Result099	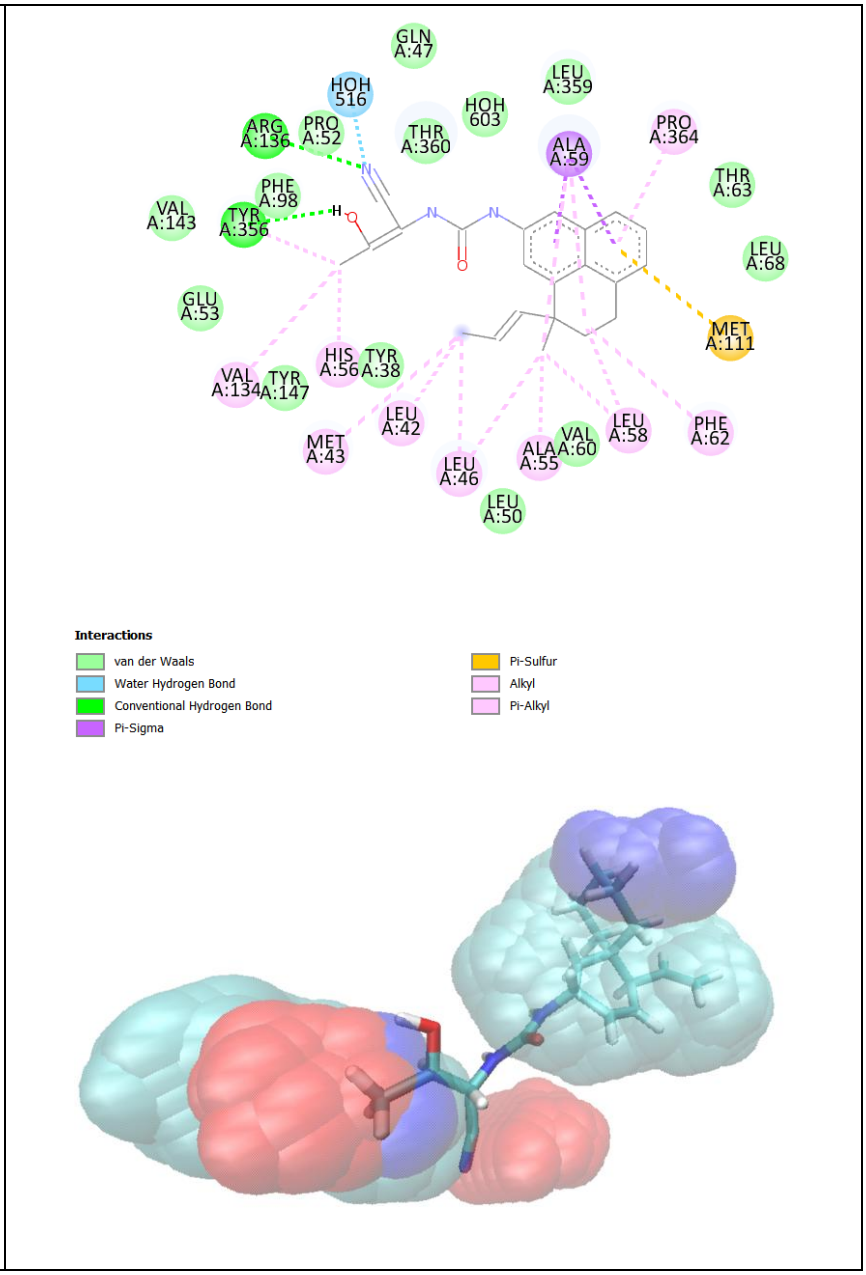

Seed33_Result103	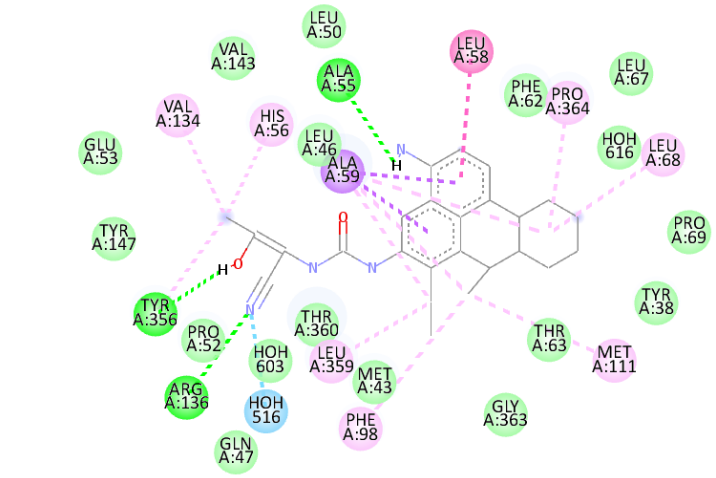  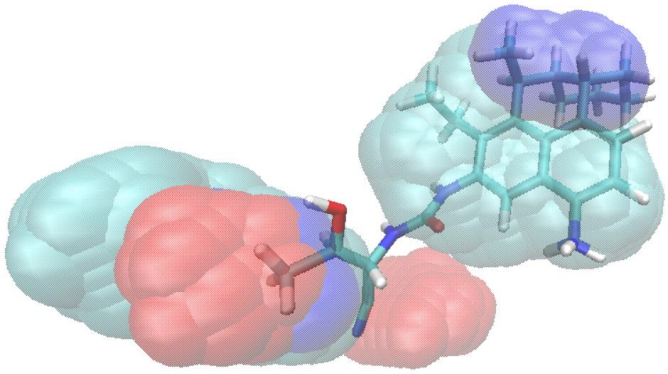

Seed33_Result199	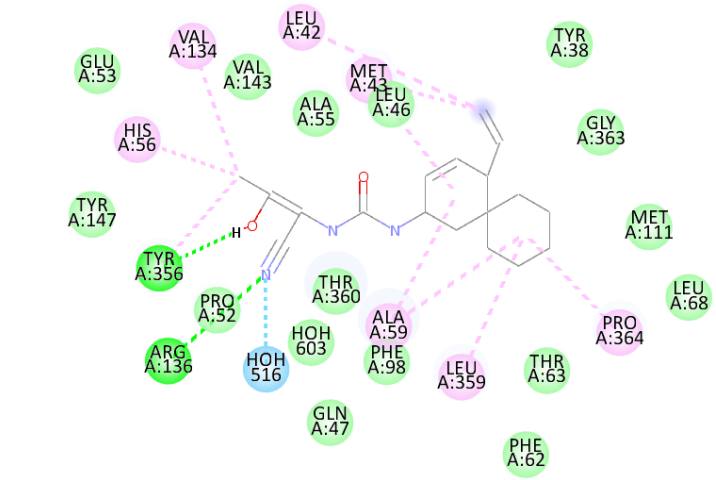 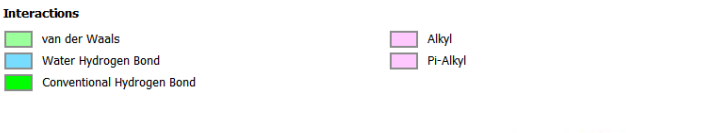 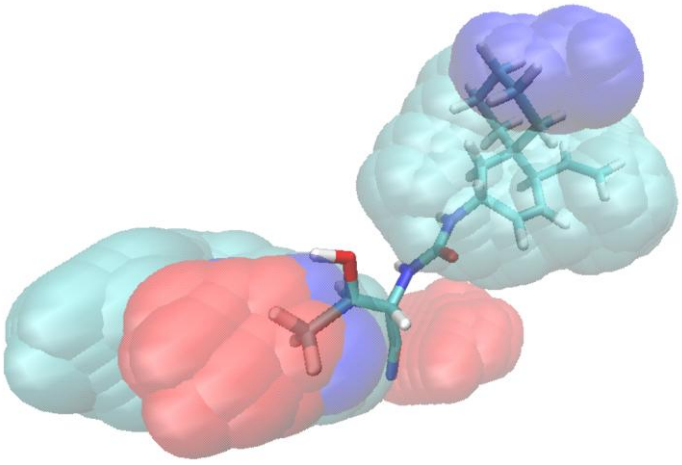

Seed34_Result194	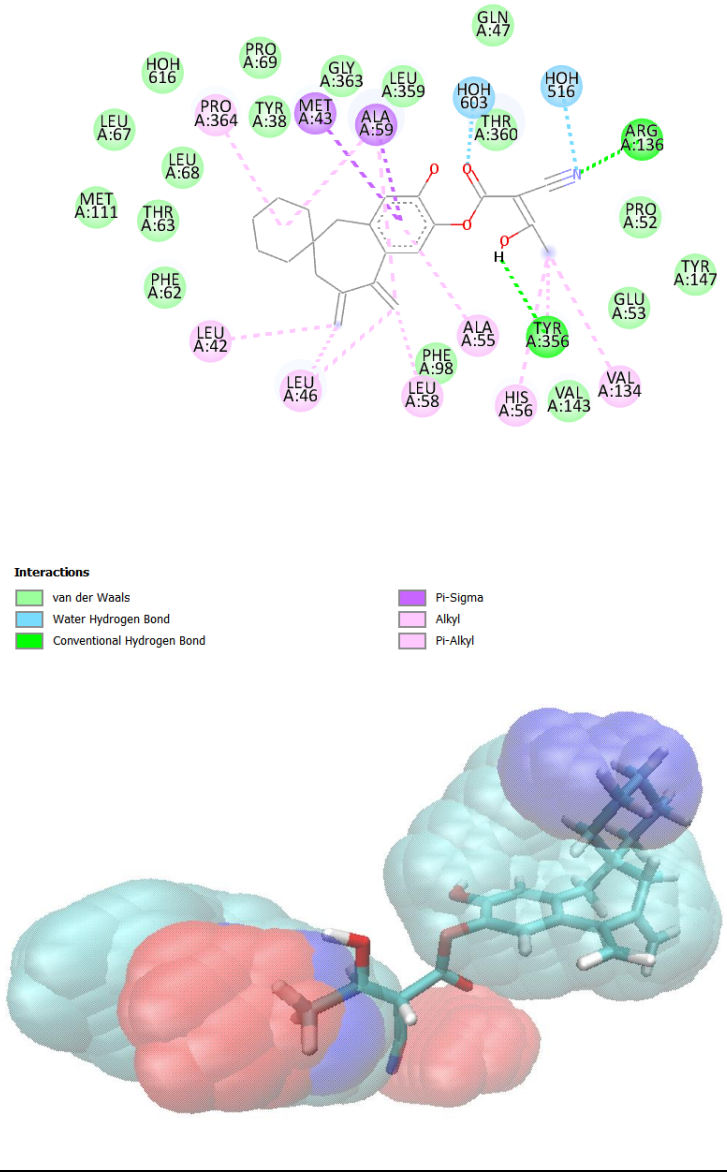

Chapter 4

Discussion

4.1 Value of the Study

The design of teriflunomide analogues was carried out by means of two different approaches to drug design, namely virtual screening and *de novo* drug design. The desired properties of the molecules designed were

- a higher degree of non-polarity compared to teriflunomide, to increase BBB penetration and bioactivity, and
- oral bioavailability.

Consequently, Lipinski's Rule of 5 (Lipinski *et al.*, 1996) and not more than 3 rotatable bonds per molecule, were set as the criteria for the selection of molecules, in order to increase the likelihood of the molecules being orally bioavailable.

Previous drug design studies on the DHODH receptor using the teriflunomide scaffold as a lead, aimed to create novel structures for use in malignant disorders (Li *et al.*, 2022; Nada *et al.*, 2023), where intra-cerebral penetration of the teriflunomide analogues is not critical, unlike in this study, where the lipophilicity of the analogues is essential to reach the site of action within in the brain to exert an anti-epileptic effect. This study also differs from those of Li *et al.* (2022) and Nada *et al.* (2023) in terms of study design. Li *et al.* (2022) used SAR data to guide the creation of novel teriflunomide analogues whereas Nada *et al.* (2023) used virtual screening. This study took drug design a step further by implementing the *de novo* drug design approach, which probed the DHODH ligand binding pocket using a series of teriflunomide-based scaffolds, creating novel analogues which may not have been created using SAR, since Li *et al.* (2022) focused on improving the inhibitory effects of the teriflunomide analogues and not on exploring unoccupied areas of the DHODH ligand

binding pocket. Moreover, the virtual screening library used by Nada *et al.* (2023) was very small as their aim was to develop analogues which were easy to synthesise using the compounds available in their laboratory. This constraint was not present in this study since the focus was on the *in silico* phase of drug design and since the ZINCPharmer® (Koes & Camacho, 2012) compound library used, contains 18.3 million commercially available compounds.

A patent (WO 2025/041128) submitted by Pessah *et al.* (2025) presents DHODH inhibitors with BBB activity, however they are not based on the teriflunomide scaffold and the drug design strategies used to develop the compounds are not outlined. Therefore, this study contributed to the development of a previously unexplored subset of DHODH inhibitors, namely teriflunomide analogues capable of intracerebral penetration, using well-established *in silico* drug design approaches hitherto not known to be used on the teriflunomide scaffold. The compounds developed have the potential to narrow the treatment gap in refractory forms of epilepsy, such as Dravet's syndrome, for which there currently is insufficient treatment, by means of a novel mode of action, namely DHODH inhibition.

4.2 Comparison of virtual screening and *de novo* drug design approaches

Two approaches to drug design were followed since they produced two different but complementary molecular cohorts, which in their entirety aim to offset the limitations of each approach. The optimal molecules selected from the virtual screening process all originated from the ZINCPharmer® Purchasable database which contains molecules which have already been synthesised, eliminating the need to design synthetic production routes (Koes & Camacho, 2012), whereas *de novo* drug design created molecules for which synthetic

routes of production may be non-existent or non-feasible (Gao & Coley, 2020). Nevertheless, virtual screening can also identify molecules which have not been synthesised yet, allowing for a large cohort of molecules to be screened, making it a useful tool when structural innovation is desired (Lin et al., 2020). Despite *de novo* drug design not being structurally innovative, it is innovative from an intellectual property perspective, as novel patentable molecules may be produced (Mouchlis *et al.*, 2021). The generation of novel molecules by means of *de novo* design complements virtual screening as a wider chemical space is explored, increasing the possibility of finding successful molecules (Tang *et al.*, 2024). *De novo* drug design, however, tends to be more time-consuming than virtual screening since all the molecules must be synthesised from scratch and since *de novo* molecules tend to be larger in size in order to achieve a higher binding affinity (Yuan *et al.*, 2011).

Both drug design approaches are efficient and cost-effective since they significantly decrease the number of molecules tested *in vitro*, as inactive molecules are discarded before synthesis (Gimeno *et al.*, 2019). The molecules created by the *de novo* approach are more likely to be bioactive since the molecules are grown inside the ligand binding pocket. Conversely, the virtual screening molecules are less likely to be bioactive since they were docked into the protomol, which is the energetically unsatisfied space within the receptor and not the bioactive site. However, growth outside the bioactive site may possibly elicit other pharmacotherapeutic responses (Zhu *et al.*, 2022), which would have to be investigated further to establish their utility. Ultimately, all molecules, whether obtained through virtual screening or *de novo* drug design, tend to be far from the final drug, however they serve as good starting points for further development (Tang *et al.*, 2024).

4.3 Analysis of Virtual Screening Results

The structure of the hits obtained depended solely on the modelled pharmacophores. A consensus pharmacophore was created since it combined several pharmacophores to give a more accurate representation of the critical moieties that bind to the target, thus facilitating the retrieval of hits with similar activity at the target (Ruiz-Moreno *et al.*, 2024). For the creation of the consensus pharmacophore, a biaryl analogue of teriflunomide was selected due to its favourable pharmacokinetic properties and since X-Ray crystallographic data on the ligand-protein complex was available, allowing for structure-based pharmacophore design, an approach which creates pharmacophores based on the key interactions between the ligand and the target protein. However, other ligands could have been selected instead of the biaryl analogue of teriflunomide, possibly leading to the generation of a different consensus pharmacophore and consequently in the retrieval of different hits from the ZINCPharmer® database. One such alternative ligand is the brain permeable DHODH inhibitor SLN-031, designed by Pessah *et al.* (2025), which would have to be docked into the DHODH receptor for prediction of the ligand-protein interactions. Despite the advantages of using a consensus pharmacophore as a query for virtual screening, it gives more importance to common features in the molecules it is based on, potentially dismissing unique moieties which may be essential to ligand binding and specificity (Ruiz-Moreno *et al.*, 2024).

The three optimal hits generated through virtual screening have similar affinities to the protomol ($4.0 < \text{Total Score} > 5.0$). A Total Score between 4.0 and 5.0 indicates that the hits exhibit some binding affinity to the protomol (Feng *et al.*, 2022). Their crash scores are negative, indicating some steric hindrance within the ligand and/or between the ligand and the DHODH receptor (Cao *et al.*, 2019). The polar scores, which form part of the total scores

for each molecule, indicate that for the three molecules selected, polar bonds such as hydrogen bonds, account for a third to half of the bonding occurring between the molecules and the DHODH receptor. The DHODH ligand binding pocket contains amino acid residues which are polar, such as Tyr^{356} and Arg^{136}, with which teriflunomide forms critical interactions, therefore, the polar score of the molecules selected shows that they also form polar bonds, which are desirable for DHODH inhibitory activity (Kujawski *et al.*, 2015). However, since the ligand binding pocket is found within the hydrophobic channel of the DHODH receptor, non-polar interactions such as van der Waals interactions are also important to stabilise the molecules (Munier-Lehmann *et al.*, 2013).

All three molecules have a clogP higher than the clogP of teriflunomide, however, the clogP of ZINC06536819 is significantly higher, being 3.45 compared to 2.14 for teriflunomide, making it a particularly good candidate for use in further studies, as it is more likely to cross the BBB to act on intracerebral DHODH receptors. Moreover, the BBB activity of the three molecules has been predicted to be active when the toxicity screening was carried out. Toxicity screening, indicated that ZINC06536819 is harmful when swallowing, showing the need for optimisation. However, in comparison, teriflunomide also has an unfavourable toxicity profile and a lower LD_{50}, suggesting that ZINC06536819 is still a promising candidate for further study. Unlike its lead molecule teriflunomide, it is not hepatotoxic or immunotoxic, indicating that virtual screening retrieved molecules with improved toxicity profiles. The toxicity of ZINC06536819 may be attributed to the presence of the polycyclic aromatic, phenol and hydrazine moieties seen in Figure 4.1.

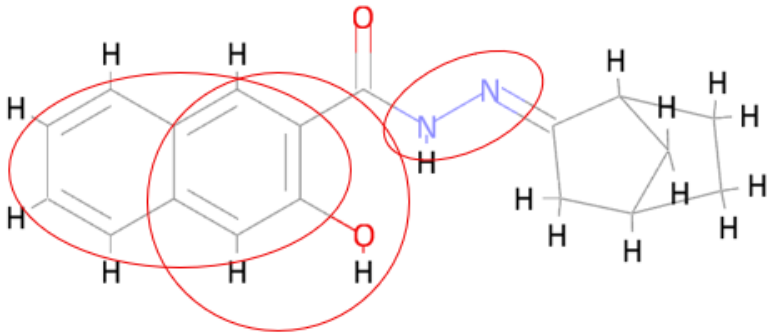

Figure 4..1 Toxiphores present on ZINC06536819, rendered in BIOVIA Draw®.[3]

Compounds ZINC73182521 and ZINC81626129 were predicted to be more toxic as they are harmful when swallowed. Figures 4.2 and 4.3 show the moieties on these molecules, which may be contributing to their toxicity profile. ZINC73182521 contains hydrazine and phenol moieties whereas ZINC81626129 contains a polyaromatic moiety.

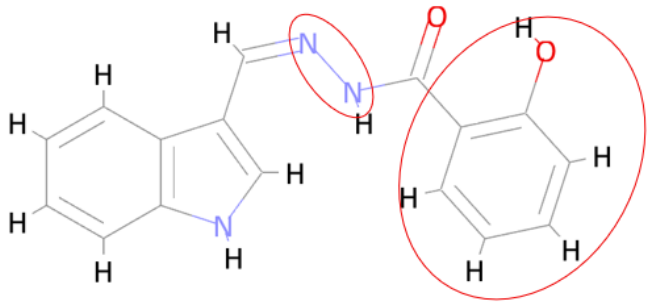

Figure 4.2 Toxiphores present on ZINC73182521, rendered in BIOVIA Draw®.[3]

[3] Dassault Systèmes. Biovia Draw®. Version 21.1 [software]. Dassault Systèmes. 2024 [cited 2025 Jul 26; downloaded 2023 Oct 19]. Available from: https://discover.3ds.com/biovia-draw-academic#_ga=2.9885366.2038323275.1652726867-4a55e360-cfd1-11ec-9db0-078235bac709.

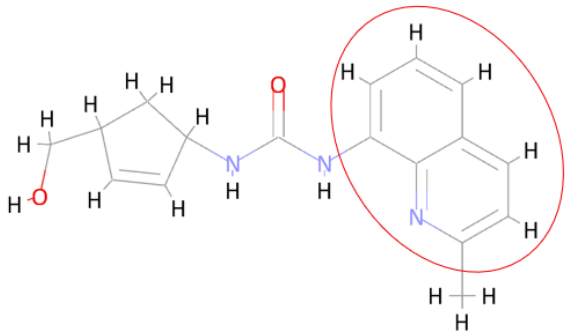

Figure 4.3 Toxiphores present on ZINC81626129, rendered in BIOVIA Draw®.[3]

Polycyclic aromatic moieties may cause toxicity through the covalent bonding of their metabolites to DNA, causing carcinogenicity (Peng *et al.*, 2023). Phenol compounds exhibit anti-oxidative properties; however high concentrations have been associated with neuro- and nephrotoxicity (de Lima Pena *et al.*, 2025). Metabolism of hydrazines may form reactive species which are mutagenic and carcinogenic (Sinha & Mason, 2014). The presence of toxiphores on a compound, do not inherently make a molecule toxic, therefore further SAR studies are required to determine whether the toxiphoric moieties identified contribute to the toxicity profiles of the molecules. In the affirmative, non-toxic bioisosteres of the toxic moieties can be used to replace them to improve toxicity, whilst retaining their binding affinities.

A comparison of the virtual screening molecules with the compounds designed by Li *et al.* (2022), Nada *et al.* (2023) and Pessah *et al.* (2025) revealed structural similarities which go beyond the teriflunomide-based moieties. The compounds designed by Li *et al.* (2022) and Nada *et al.* (2023) have multiple aromatic rings, similar to the virtual screening molecules.

[3] Dassault Systèmes. Biovia Draw®. Version 21.1 [software]. Dassault Systèmes. 2024 [cited 2025 Jul 26; downloaded 2023 Oct 19]. Available from: https://discover.3ds.com/biovia-draw-academic#_ga=2.9885366.2038323275.1652726867-4a55e360-cfd1-11ec-9db0-078235bac709.

A five-membered ring, occasionally substituted with a nitrogen atom, is present on all the virtual screening molecules and molecules developed by Nada *et al.* (2023) and Pessah *et al.* (2025), suggesting the importance of these moieties for DHODH inhibition. All the molecules developed by the aforementioned researchers are fluorinated, unlike the virtual screening molecules, indicating that when optimisation is carried out, the effect of a fluorine substitution on aromatic rings should be investigated.

The three molecules follow the Rule of 3 for lead likeness (Congreve *et al.*, 2003) with respect to molecular weight and number of rotatable bonds, allowing for optimisation to be done without violating Lipinski's Rule of 5 (Lipinski *et al.*, 1996). If necessary, some hydrogen bond donors and acceptors can be added without violating Lipinski's Rule of 5 (Lipinski *et al.*, 1996). However, moieties creating van der Waals interactions are preferred, as they increase the binding affinity of the molecules to the receptor whilst retaining Lipinski Rule of 5 (Lipinski *et al.*, 1996) compliance.

4.4 Analysis of *de novo* drug design results

Structure-based *de novo* drug design was employed since the 3D structure of the DHODH receptor is known (through X-Ray crystallography), allowing for the analysis of the interactions between the lead molecule teriflunomide and the active site of the DHODH receptor (Mouchlis *et al.*, 2021). Fragment-based design of novel molecules was chosen over atom-based design since the former, albeit generating less structures, results in molecules with better synthetic accessibility and better absorption, distribution, metabolism, excretion and toxicity (ADMET) properties (Devi *et al.*, 2015). The fragments designed aimed to include the teriflunomide-DHODH interactions (derived from the 2D topology map) deemed

to be essential to binding, namely hydrogen bond interactions with amino acid residues Tyr^{356} and Arg^{136} (Kujawski *et al.*, 2015).

The atomic binding score of each atom on the teriflunomide scaffold also provided SAR data on which atoms are critical for binding within the DHODH ligand binding pocket. The aromatic ring, the methyl group and the hydroxyl group are the main contributors to the total binding affinity. The importance of an aromatic ring inside the ligand binding pocket is highlighted by the structures created by means of *de novo* drug design, of which five of the structures grown have an aromatic ring despite the moiety not being part of the seed structure. Only one of the d*e novo* molecules does not have an aromatic ring, which may account for the lower binding affinity to the DHODH ligand binding pocket in comparison to the other molecules generated. In view of the importance of the aromatic ring to the binding affinity of teriflunomide to the DHODH ligand binding pocket, seeds based on the aromatic ring were also designed. However, these did not grow within the ligand binding pocket. This may be attributed to the 4-trifluoromethyl moiety which despite increasing DHODH activity (Li *et al.*, 2022), is strongly electronegative, resulting in steric hindrance which may affect the attachment of substituents on the adjacent aromatic ring (Yi *et al.*, 2020).

Seed 30 (methyl group of teriflunomide) was designed since the methyl group was determined to be a main contributor to the total binding affinity of teriflunomide in X-Score® (Wang *et al.*, 2002). Based on the 2D topology map created for teriflunomide, the moiety constituting Seed 30 does not form critical interactions with amino acid residues Tyr^{356} and Arg^{136} within the DHODH ligand binding pocket by means of hydrogen bonding. However, the *de novo* molecules derived from it (Seed30_Result195 and Seed30_Result196), do form interactions with these amino acid residues, albeit in the form of van der Waals and alkyl

interactions, which are weaker than hydrogen bond interactions, but contribute to ligand-target stability (Ferenczy & Kellermayer, 2022). Since it is hydrogen bonds and not hydrophobic interactions which impart specificity to the binding of a ligand to its target (Bissantz *et al.*, 2010), the extent of DHODH inhibition by the molecules derived from Seed 30 is must be determined.

Seeds 33 and 34 were designed since their constituents form critical interactions with Tyr^{356} and Arg^{136} within the DHODH ligand binding pocket. The *de novo* molecules generated using these seeds all interact with the two critical amino acid residues by means of hydrogen bonding, which makes them more likely to bind with specificity to their target to cause DHODH inhibition (Bissantz *et al.*, 2010). In addition, they form ligand-target stabilising hydrophobic contacts such as van der Waals, Pi Sigma and alkyl interactions through their aliphatic and aromatic ring constituents.

The superimposition of 3D renders of all the six *de novo* molecules within the DHODH ligand binding pocket indicate that the hydrophobic contacts enable the molecules to probe the ligand binding pocket more extensively compared to teriflunomide. However, as shown in Figure 4.4, there remain areas of the ligand binding pocket (circled in yellow) which have not been explored by the *de novo* molecules generated.

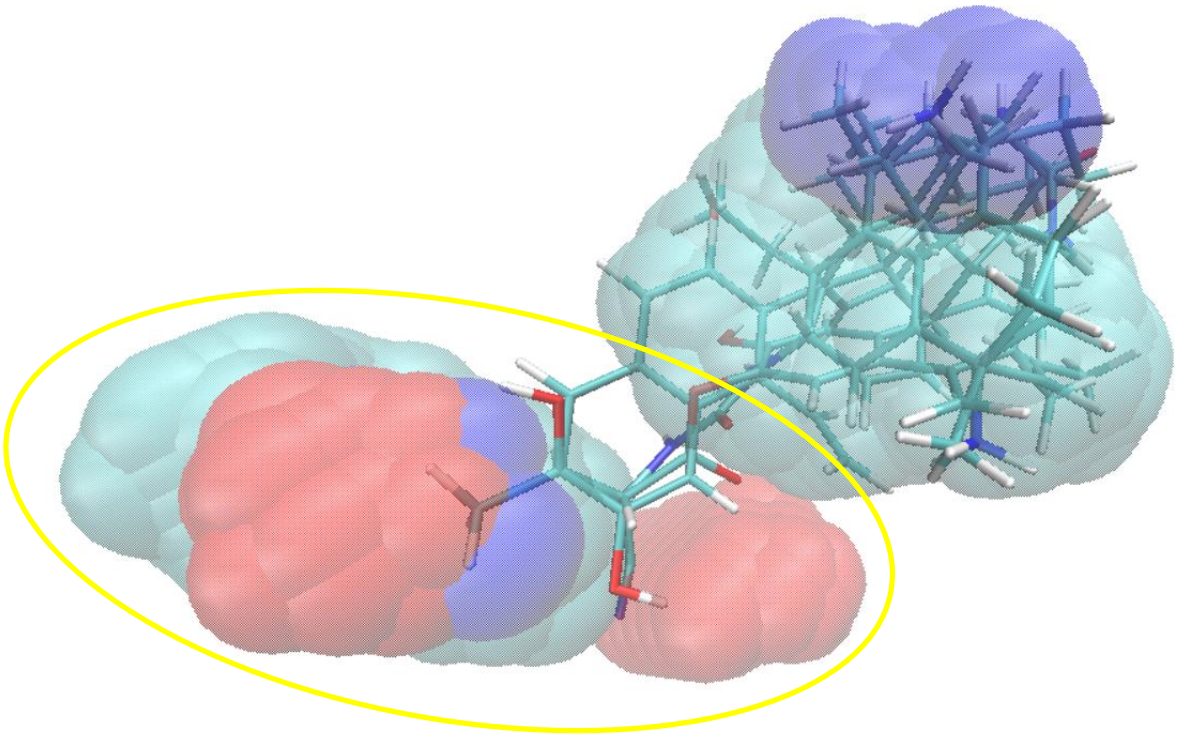

Figure 4.4 Visualisation of the DHODH ligand binding pocket, with all the *de novo* molecules superimposed, as rendered in VMD® (Humphrey *et al.*, 1996). The hydrophobic areas are depicted in green, the hydrogen bond donors in blue and the hydrogen bond acceptors in red.

Optimisation may be focussed on probing these areas. For most of the molecules, more hydrogen bond donors and acceptors can be added, whilst retaining Lipinski Rule of 5 compliance (Lipinski *et al.*, 1996). The addition of such polar moieties is likely to be unavoidable since two hydrogen bond acceptor areas and one hydrogen bond donor area of the DHODH ligand binding pocket are unexplored by the molecules. The molecular weights of the molecules are also well below the limit of 500 Daltons, allowing the addition of non-polar moieties to probe the unexplored hydrophobic area of the ligand binding pocket.

The binding affinity of the *de novo* molecules, despite being for the DHODH ligand binding pocket, is not necessarily representative of the binding affinity *in vivo*, since the conformations adopted by the molecules for the calculation are not necessarily the bioactive conformations. This also applies for the virtual screening molecules as their binding affinity is for the protomol and not for the ligand binding pocket. Secondly, *de novo* drug design tools tend to design large molecules to achieve a higher binding activity, without consideration of maintaining critical interactions and shape complementarity between the protein and the ligand (Yuan *et al.*, 2011).

The compounds generated through *de novo* drug design all have a clogP higher than teriflunomide and higher than the clogP of the virtual screening hits, indicating that they are more likely to cross the BBB. Toxicity predictions confirmed that all six compounds are active on the BBB. Five of them are toxic or harmful if swallowed, requiring optimisation to improve their toxicity profiles. Compound Seed 33_Result199, however, is non-toxic if swallowed (Toxicity Class 6). The toxicity class indicates the acute toxicity of the compound in a rodent when administered over a span of less than 24 hours (Banerjee *et al.*, 2024). Therefore, the effects in humans and the longterm toxic effects still must be determined to establish whether the compound is truly non-toxic. When comparing the hepatotoxic and immunotoxic properties of the *de novo* molecules to the parent molecule teriflunomide, Seed33_Result103, Seed33_Result199 and Seed34_Result194 did not exhibit toxicity in these domains, unlike teriflunomide. Seed34_Result199 has a significantly higher LD_{50} than all the other molecules, except for Seed33_Result199, and the highest binding affinity for the DHODH ligand binding pocket, indicating that it shows promise for further optimisation.

However, this does not exclude the other molecules from further studies, since optimisation and docking of the molecules may change their properties and suitability as drug molecules.

Figures 4.5 and 4.6 show the polyaromatic, phenolic and conjugated alkene moieties on Seed30_Result195 and Seed 30_Result196, which may be contributing to their toxicity classification.

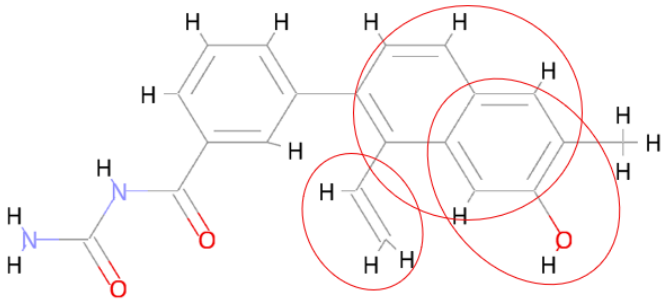

Figure 4.5 Toxiphores present on Seed30_Result195, rendered in BIOVIA Draw®.[3]

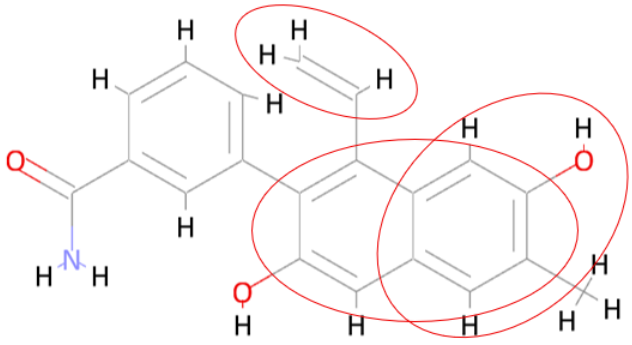

Figure 4.6 Toxiphores present on Seed30_Result196, rendered in BIOVIA Draw®.[3]

[3] Dassault Systèmes. Biovia Draw®. Version 21.1 [software]. Dassault Systèmes. 2024 [cited 2025 Jul 26; downloaded 2023 Oct 19]. Available from: https://discover.3ds.com/biovia-draw-academic#_ga=2.9885366.2038323275.1652726867-4a55e360-cfd1-11ec-9db0-078235bac709.

Figures 4.7 and 4.8 show the potentially toxic groups on Seed33_Result099 and Seed33_Result103, namely the alkene, polyaromatic and aryl amine moieties.

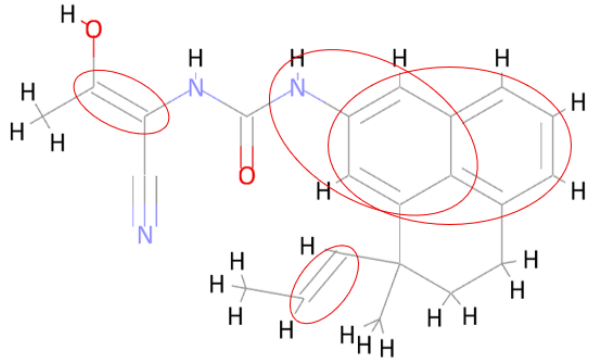

Figure 4.7 Toxiphores present on Seed33_Result099, rendered in BIOVIA Draw®.[3]

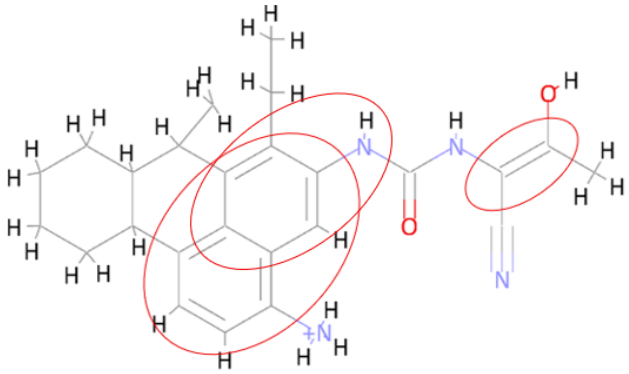

Figure 4.8 Toxiphores present on Seed33_Result103, rendered in BIOVIA Draw®.[3]

[3] Dassault Systèmes. Biovia Draw®. Version 21.1 [software]. Dassault Systèmes. 2024 [cited 2025 Jul 26; downloaded 2023 Oct 19]. Available from: https://discover.3ds.com/biovia-draw-academic#_ga=2.9885366.2038323275.1652726867-4a55e360-cfd1-11ec-9db0-078235bac709.

Figure 4.9 highlights the potentially toxic alkene moieties present on Seed33_Result199.

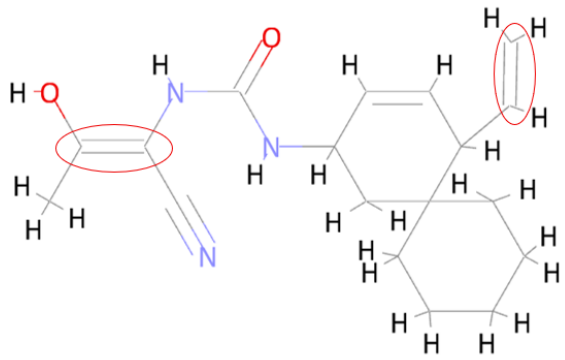

Figure 4.9 Toxiphores present on Seed33_Result199, rendered in BIOVIA Draw®.[3]

Figure 4.10 highlights the potentially toxic alkene and phenol moieties present on Seed34_Result194.

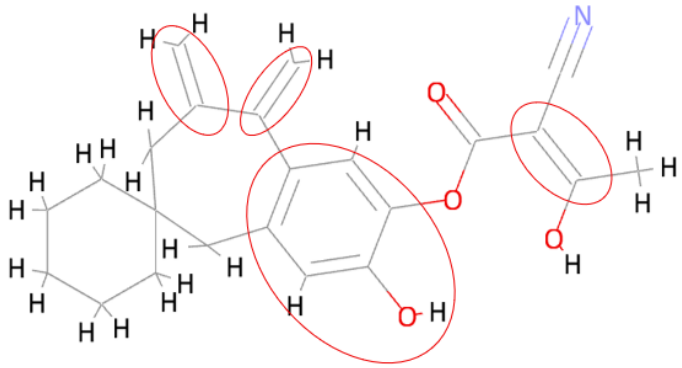

Figure 4.10 Toxiphores present on Seed34_Result194, rendered in BIOVIA Draw®.[3]

The toxicities of the polyaromatic, phenol and hydrazine moieties were discussed previously. Alkene moieties can undergo epoxidation reactions by CYP 450 enzymes, resulting in hepatotoxic and carcinogenic metabolites (Zhang *et al.*, 2016). Aryl amine groups may

[3] Dassault Systèmes. Biovia Draw®. Version 21.1 [software]. Dassault Systèmes. 2024 [cited 2025 Jul 26; downloaded 2023 Oct 19]. Available from: https://discover.3ds.com/biovia-draw-academic#_ga=2.9885366.2038323275.1652726867-4a55e360-cfd1-11ec-9db0-078235bac709.

impart toxicity to a molecule through oxidation to form reactive metabolites which are carcinogenic and haematotoxic (Siraki, 2013).

The molecules grown from Seed 30 have a good synthetic accessibility score (2.58), indicating that they are relatively easily to synthesise, whilst the molecules grown from Seeds 33 and 34 are either more difficult to synthesise, or no synthetic accessibility score could be computed. LigBuilder® (Yuan *et al.*, 2011) makes use of retrosynthetic analysis to guide the generation of molecules which are as easy to synthesise as possible, by transforming the generated molecules into simpler precursor structures until simple and commercially available starting structures are obtained. Furthermore, the fragment library of LigBuilder® (Yuan *et al.*, 2011), on which the molecules are based, consists of synthesisable and drug-like fragments.

Comparing the *de novo* molecules obtained to the molecules designed by Li *et al.* (2022), Nada *et al.* (2023) and Pessah *et al.* (2025), the same observations made in the comparison for the virtual screening molecules can be concluded. Additionally, the molecules synthesised by the other researchers have typically have polar substitutions on all aliphatic and aromatic rings, whilst still being orally bioavailable, which further emphasises the importance of optimising the *de novo* molecules using polar groups, to better occupy the DHODH ligand binding pocket.

4.5 Comparison of virtual screening and *de novo* drug design results

The principal difference between the virtual screening and the *de novo* drug design molecules is the molecular weight cutoff used to generate them. For virtual screening, the Rule of 3 (Congreve *et al.*, 2003) was applied with respect to molecular weight whereas for *de novo*

drug design the Rule of 5 (Lipinski *et al.*, 1996) was applied. The lower molecular weight of the virtual screening molecules allows for them to be more easily optimised whilst still retaining Lipinski Rule compliance. This was not applied to the *de novo* molecules since a restricted filter results in less molecules being generated.

The differing molecular weight cutoffs also contributed to the virtual screening molecules being less lipophilic than the *de novo* molecules. All the molecules have similar hydrogen bond donor and acceptor counts, indicating that hydrophobic groups account for the additional molecular weight of the *de novo* molecules when compared to the virtual screening molecules, which in turn increases their lipophilicity (Lipinski *et al.*, 1996).

The binding affinities of the *de novo* molecules produced cannot be directly compared to the binding affinities of the virtual screening molecules. The binding affinity computed for the *de novo* molecules is an indication of the affinity to the DHODH ligand binding pocket, whereas the binding affinity computed for the virtual screening molecules is an indication of the affinity to the protomol, the two entities not being identical.

4.6 Limitations

The general limitations of each drug design method have already been outlined in a comparative approach. Nonetheless, there exist study design limitations, some of which could be reduced or overcome in further work carried out on the findings of this study.

For virtual screening, only the ZINCPharmer® molecule databases were searched, which were last updated in 2014. Using other molecular databases such as PubChem could have increased the number of hits obtained.[6]

The 35 seed structures created for *de novo* drug design do not comprise an exhaustive list of the possible seed structures that can be derived from teriflunomide. Consequently, seed structures which would have sustained growth within the DHODH ligand binding pocket may not have been designed and included in this study. LigBuilder® (Yuan *et al.*, 2011) has an automatic extractor which can be used for the generation of a more comprehensive library of seed structures.

The binding affinities of the molecules chosen, as calculated by SYBYL-X® (Ash *et al.*, 2010) and LigBuilder® (Yuan *et al.*, 2011), are not necessarily representative of the binding affinities *in vivo*. More accurate binding affinity values can be obtained by docking the molecules into their receptor using a docking programme which predicts the most favourable conformation for a molecule to bind to its target, taking into account the ligand-interactions and conformational energies, and then rescoring the binding affinities. Similarly, the 2D topology maps for the *de novo* molecules should be regenerated using the best conformations docked into the ligand binding pocket, to determine the most likely receptor ligand-interactions present *in vivo*.

Lipinski's Rule of 5 (Lipinski *et al.*, 1996) and the Rule of 3 (Congreve *et al.*, 2003) with respect to rotatable bond count were used as filters for the selection of orally bioavailable molecules. Other studies (Muegge *et al.*, 2001; Veber *et al.*, 2002) suggest that the polar

[6] National Library of Medicine (NLM). PubChem [Internet]. Maryland (USA): NLM; 2025 [cited 2025 Aug 3]. Available from: https://pubchem.ncbi.nlm.nih.gov/compound/54684141.

surface area and number of rotatable bonds are better predictors of oral bioavailability than the molecular weight filter. Lipophilicity is an important factor contributing to drug-likeness, as it affects passive membrane diffusion and plasma protein binding, however parameters other than clogP, such as logD and ligand lipophilicity efficiency, may describe it better (Caminero Gomes Soares *et al.*, 2023). As a result, the use of the Rule of 5 heuristic may have filtered off some promising molecules unnecessarily. This could be mitigated by applying other oral bioavailability rules (Egan *et al.*, 2000; Muegge *et al.*, 2001; Veber *et al.*, 2002) in conjunction with Lipinski's Rule of 5 (Lipinski *et al.*, 1996).

The primary limitation of this study is that both the ligands and the target were treated as static entities, which is not the case *in vivo*. For this purpose, molecular dynamics studies should be carried out to determine how conformational changes, ligand binding and protein folding impact the inhibitory effect of the ligands on the DHODH target receptor. Molecular dynamics studies can also be carried out in different conditions, to better simulate the *in vivo* environment (Hollingsworth & Dror, 2018). Water molecules and ions, which were present in the PDB crystallographic depositions used in this study, often contribute to the modulation of ligand binding (Betz *et al.*, 2016). Their effect was not evaluated in this study, demonstrating the importance of carrying out molecular dynamics studies using the molecules designed.

4.7 Recommendations for Further Study

Listed in order of importance are some areas of further work which can be carried out on the findings of the study.

i. Use of artificial intelligence (AI)

   AI integrated software such as PharmAI DiscoveryEngine® (Gryniukova *et al.*, 2023) can be used for virtual screening and Chemistry 42® (Ivanenkov *et al.*, 2023) can be used for *de novo* design and optimisation. AI enables the rapid screening of large molecular/fragment libraries, increasing the number and structural novelty of the molecules generated (Qu *et al.*, 2023).

ii. Pan-Assay INterference compounds (PAINs) filtering

   PAINs filtering enables the elimination of molecules which interfere with biochemical assays, thus reducing the time spent on optimising molecules unlikely to develop into useful compounds (Baell & Nissink, 2018).

iii. Molecular docking

   Docking programmes such as SwissDock® (Bugnon *et al.*, 2024) can be used to determine the optimal conformations of the molecules.

iv. Molecular dynamics simulations

   Software packages such as CP2K® (Kühne *et al.*, 2020) can be used to simulate *in vivo* conditions.

v. Optimisation of the molecules

   Optimisation is done to enhance the specificity of a molecule for the target receptor, to reduce toxicity and to maintain or increase potency. This can be done by means of bioisosteric replacement which replaces parts of a molecule with fragments to create

a similar compound with improved properties. Usually, the side-chains of a molecule are replaced (Cuozzo *et al.*, 2022). The 2D topology maps and the calculation of the atomic binding score of individual atoms can be used to identify the areas of the molecules where optimisation can be carried out. SAR studies can also be conducted.

vi. Development of synthetic routes for the *de novo* design compounds.

The synthetic accessibility scores of the molecules designed indicate predict that they are not challenging to synthesise. This can be proven using retrosynthetic planning software such as AiZynthFinder® (Genheden *et al.*, 2020), which identifies reaction pathways for commercially available compounds from which the molecules can be then synthesised.

vii. *In vitro* testing

The molecular docking studies can be validated by means of *in vitro* tests such as binding assays, functional assays and selectivity evaluation, which determine the binding affinity and biological effects of the molecules at the DHODH target enzyme and whether the molecules exhibit any activity at non-cognate receptors (Tang *et al.*, 2024).

viii. *In vivo* testing

In vivo testing is carried out to determine the pharmacokinetic and toxicological properties of the drug-like molecules (Tang *et al.*, 2024). Teriflunomide has a long half-life and teratogenic properties, therefore it is important to evaluate these parameters in its analogues to determine whether they are suitable in pregnancy (Varytė *et al.*, 2021).

4.8 Conclusions

This study proposed novel DHODH inhibitors based on the teriflunomide scaffold, which are more non-polar than teriflunomide. This enhances BBB penetration, with the purpose of exerting an anti-epileptic effect through intracerebral DHODH inhibition. The molecules were identified through virtual screening or generated by means of *de novo* drug design, with application of Lipinski's Rules for oral bioavailability (Lipinski *et al.*, 1996) and the Rule of 3 (Congreve *et al.*, 2003) with respect to rotatable bond count. The most promising molecules will undergo molecular dynamics simulations and optimisation.

References

Alamri RD, Elmeligy MA, Albalawi GA, Alquayr SM, Alsubhi SS, El-Ghaiesh SH. Leflunomide an immunomodulator with antineoplastic and antiviral potentials but drug-induced liver injury: A comprehensive review. Int Immunopharmacol. 2021;93(1):107398. doi: 10.1016/j.intimp.2021.107398.

Ash S, Cline MA, Homer RW, Hurst T, Smith GB. SYBYL Line Notation (SLN): A Versatile Language for Chemical Structure Representation. ChemInform. 2010;28(18):66-78. doi: 10.1002/chin.199718282.

Baell JB, Nissink JWM. Seven Year Itch: Pan-Assay Interference Compounds (PAINS) in 2017—Utility and Limitations. ACS Chem Biol. 2018;13(1):36–44. doi: 10.1021/acschembio.7b00903.

Banerjee P, Kemmler E, Dunkel M, Preissner R. ProTox 3.0: a webserver for the prediction of toxicity of chemicals. Nucleic Acids Res. 2024;52(W1):W513–20. doi: 10.1093/nar/gkae303.

Betz M, Wulsdorf T, Krimmer SG, Klebe G. Impact of Surface Water Layers on Protein–Ligand Binding: How Well Are Experimental Data Reproduced by Molecular Dynamics Simulations in a Thermolysin Test Case? J Chem Inf Model. 2016;56(1):223–33. doi: 10.1021/acs.jcim.5b00621.

Biolato M, Bianco A, Lucchini M, Gasbarrini A, Mirabella M, Grieco A. The Disease-Modifying Therapies of Relapsing-Remitting Multiple Sclerosis and Liver Injury: A Narrative Review. CNS Drugs. 2021;35(8):861–80. doi: 10.1007/s40263-021-00842-9.

Bissantz C, Kuhn B, Stahl M. A Medicinal Chemist's Guide to Molecular Interactions. J Med Chem. 2010;53(14):5061–84. doi: 10.1021/jm100112j.

Boncristiano A, Balestrini S, Doccini V, Specchio N, Pietrafusa N, Trivisano M, et al. Fenfluramine treatment for Dravet syndrome: Long term real-world analysis demonstrates safety and reduced health care burden. Epilepsia. 2025;66(4):1110–8. doi: 10.1111/epi.18241.

Bugnon M, Röhrig UF, Goullieux M, Perez MAS, Daina A, Michielin O, et al. SwissDock 2024: major enhancements for small-molecule docking with Attracting Cavities and AutoDock Vina. Nucleic Acids Res. 2024;52(W1):W324–32. doi: 10.1093/nar/gkae300.

Caminero Gomes Soares A, Marques Sousa G, Calil RL, Goulart Trossini G. Absorption matters: A closer look at popular oral bioavailability rules for drug approvals. Mol Inform. 2023;42(11):e202300115. doi: 10.1002/minf.202300115.

Cao L, Weetall M, Trotta C, Cintron K, Ma J, Kim MJ, et al. Targeting of Hematologic Malignancies with PTC299, A Novel Potent Inhibitor of Dihydroorotate Dehydrogenase with Favorable Pharmaceutical Properties. Mol Cancer Ther. 2019;18(1):3–16. doi: 10.1158/1535-7163.MCT-18-0863.

Congreve M, Carr R, Murray C, Jhoti H. A 'Rule of Three' for fragment-based lead discovery? Drug Disc Today. 2003;8(19):876-7. doi: 10.1016/s1359-6446(03)02831-9.

Cross JH, Caraballo RH, Nabbout R, Vigevano F, Guerrini R, Lagae L. Dravet syndrome: Treatment options and management of prolonged seizures. Epilepsia. 2019;60(3):39–48. doi: 10.1111/epi.16334.

Cuozzo A, Daina A, Perez MAS, Michielin O, Zoete V. SwissBioisostere 2021: updated structural, bioactivity and physicochemical data delivered by a reshaped web interface. Nucleic Acids Res. 2022;50(1):D1382–90. doi: 10.1093/nar/gkab1047.

Daina A, Michielin O, Zoete V. SwissADME: a free web tool to evaluate pharmacokinetics, drug-likeness and medicinal chemistry friendliness of small molecules. Sci Rep. 2017;7(1):42717. doi: 10.1038/srep42717.

de Lima Pena F, de Souza MC, Sanches VT, Viganó J, Mancini MC, Brito-Oliveira TC, et al. Phenolic profile, bioactivity and cytotoxicity of plant extracts from thyme, ginger, garlic, ground roasted coffee and coffee silverskin. Int J Food Prop. 2025;28(1):2519843. doi: 10.1080/10942912.2025.2519843.

Devi RV, Sathya SS, Coumar MS. Evolutionary algorithms for de novo drug design – A survey. Appl Soft Comput. 2015;27(1):543–52. doi: 10.1016/j.asoc.2014.09.042.

Egan WJ, Merz KM, Baldwin JJ. Prediction of Drug Absorption Using Multivariate Statistics. J Med Chem. 2000;43(21):3867–77. doi: 10.1021/jm000292e.

Eltze C, Alshehhi S, Ghfeli AA, Vyas K, Saravanai-Prabu S, Gusto G, et al. The use of cannabidiol in patients with Lennox-Gastaut syndrome and Dravet syndrome in the UK Early Access Program: A retrospective chart review study. Epilepsy Behav Rep. 2025;29(1):100731. doi: 10.1016/j.ebr.2024.100731.

Erra M, Moreno I, Sanahuja J, Andrés M, Reinoso RF, Lozoya E, et al. Biaryl analogues of teriflunomide as potent DHODH inhibitors. Bioorg Med Chem Lett. 2011;21(24):7268–72. doi: 10.1016/j.bmcl.2011.10.052.

Feng S, Wang T, Fan L, An X, Ding X, Wang M, et al. Exploring the potential therapeutic effect of Eucommia ulmoides-Dipsaci Radix herbal pair on osteoporosis based on network pharmacology and molecular docking technology. RSC Adv. 2022;12(4):2181–95. doi: 10.1039/d1ra05799e.

Ferenczy GG, Kellermayer M. Contribution of hydrophobic interactions to protein mechanical stability. Comput Struct Biotechnol J. 2022;20(1):1946–56. doi: 10.1016/j.csbj.2022.04.025.

Gao W, Coley CW. The Synthesizability of Molecules Proposed by Generative Models. Journal of Chemical Information and Modelling. 2020;60(12):5714–23. doi: 10.1021/acs.jcim.0c00174.

Gaurav A, Gautam V. Structure-based three-dimensional pharmacophores as an alternative to traditional methodologies. J Recept Ligand Channel Res. 2014;7(1):27–38. doi: 10.2147/JRLCR.S46845.

Genheden S, Thakkar A, Chadimová V, Reymond JL, Engkvist O, Bjerrum E. AiZynthFinder: a fast, robust and flexible open-source software for retrosynthetic planning. J Cheminformatics. 2020;12(1):70. doi: 10.1186/s13321-020-00472-1.

Gimeno A, Ojeda-Montes MJ, Tomás-Hernández S, Cereto-Massagué A, Beltrán-Debón R, Mulero M, et al. The Light and Dark Sides of Virtual Screening: What Is There to Know? Int J Mol Sci. 2019;20(6):1375. doi: 10.3390/ijms20061375.

Gryniukova A, Kaiser F, Myziuk I, Alieksieieva D, Leberecht C, Heym PP, et al. AI-Powered Virtual Screening of Large Compound Libraries Leads to the Discovery of Novel Inhibitors of Sirtuin-1. J Med Chem. 2023;66(15):10241–51. doi: 10.1021/acs.jmedchem.3c00128.

Habgood M. Bioactive focus in conformational ensembles: a pluralistic approach. J Comput - Aided Mol Des. 2017;31(12):1073–83. doi: 10.1007/s10822-017-0089-3.

Hilbig M, Rarey M. MONA 2: A Light Cheminformatics Platform for Interactive Compound Library Processing. J Chem Inf Model. 2015;55(10):2071–8. doi: 10.1021/acs.jcim.5b00292.

Hollingsworth SA, Dror RO. Molecular dynamics simulation for all. Neuron. 2018;99(6):1129–43. doi: 10.1016/j.neuron.2018.08.011.

Humphrey W, Dalke A, Schulten K. VMD: Visual molecular dynamics. J Mol Graph. 1996;14(1):33–8. doi: 10.1016/0263-7855(96)00018-5.

Ivanenkov YA, Polykovskiy D, Bezrukov D, Zagribelnyy B, Aladinskiy V, Kamya P, et al. Chemistry42: An AI-Driven Platform for Molecular Design and Optimization. J Chem Inf Model. 2023;63(3):695–701. doi: 10.1021/acs.jcim.2c01191.

Knupp KG, Wirrell EC. Treatment Strategies for Dravet Syndrome. CNS Drugs. 2018;32(4):335–50. doi: 10.1007/s40263-018-0511-y.

Koes DR, Camacho CJ. ZINCPharmer: pharmacophore search of the ZINC database. Nucleic Acids Res. 2012;40(1):W409-414. doi: 10.1093/nar/gks378.

Kühne TD, Iannuzzi M, Del Ben M, Rybkin VV, Seewald P, Stein F, et al. CP2K: An electronic structure and molecular dynamics software package - Quickstep: Efficient and

accurate electronic structure calculations. J Chem Phys. 2020;152(19). doi: 10.1063/5.0007045.

Kujawski J, Bernard MK, Jodłowska E, Czaja K, Drabińska B. On the interactions of leflunomide and teriflunomide within receptor cavity--NMR studies and energy calculations. J Mol Model. 2015;21(5):105. doi: 10.1007/s00894-015-2643-z.

Li C, Zhou Y, Xu J, Zhou X, Huang Z, Zeng T, et al. A novel series of teriflunomide derivatives as orally active inhibitors of human dihydroorotate dehydrogenase for the treatment of colorectal carcinoma. Eur J Med Chem. 2022;238(1):114489. doi: 10.1016/j.ejmech.2022.114489.

Li Y, Dai S, Deng Q, Liu Z. The impact and adherence of ketogenic dietary therapies for Dravet syndrome: A systematic review and meta-analysis. Seizure Eur J Epilepsy. 2025;130(1):16–24. doi: 10.1016/j.seizure.2025.05.001.

Lin X, Li X, Lin X. A Review on Applications of Computational Methods in Drug Screening and Design. Molecules. 2020;25(6):1375. doi: 10.3390/molecules25061375.

Lipinski CA, Lombardo F, Dominy BW, Feeney PJ. Experimental and computational approaches to estimate solubility and permeability in drug discovery and development settings. Adv Drug Deliv Rev. 1996;64(1):4–17. doi: 10.1016/j.addr.2012.09.019.

Liu S, Neidhardt EA, Grossman TH, Ocain T, Clardy J. Structures of human dihydroorotate dehydrogenase in complex with antiproliferative agents. Structure. 2000;8(1):25–33. doi: 10.1016/S0969-2126(00)00077-0.

Mei D, Cetica V, Marini C, Guerrini R. Dravet syndrome as part of the clinical and genetic spectrum of sodium channel epilepsies and encephalopathies. Epilepsia. 2019;60(3):2–7. doi: 10.1111/epi.16054.

Mouchlis VD, Afantitis A, Serra A, Fratello M, Papadiamantis AG, Aidinis V, et al. Advances in De Novo Drug Design: From Conventional to Machine Learning Methods. Int J Mol Sci. 2021;22(4):1676. doi: 10.3390/ijms22041676.

Muegge I, Heald SL, Brittelli D. Simple Selection Criteria for Drug-like Chemical Matter. J Med Chem. 2001;44(12):1841–6. doi: 10.1021/jm015507e.

Munier-Lehmann H, Vidalain P-O, Tangy F, Janin YL. On Dihydroorotate Dehydrogenases and Their Inhibitors and Uses. J Med Chem. 2013;56(8):3148–67. doi: 10.1021/jm301848w.

Nada H, Kim S, Park S, Lee MY, Lee K. Identification of Potent hDHODH Inhibitors for Lung Cancer via Virtual Screening of a Rationally Designed Small Combinatorial Library. ACS Omega. 2023;8(24):21769–80. doi: 10.1021/acsomega.3c01323.

Peng B, Dong Q, Li F, Wang T, Qiu X, Zhu T. A Systematic Review of Polycyclic Aromatic Hydrocarbon Derivatives: Occurrences, Levels, Biotransformation, Exposure Biomarkers, and Toxicity. Environ Sci Technol. 2023;57(41):15314–35. doi: 10.1021/acs.est.3c03170.

Pessah N, Getter T, Mostinski Y, Bingor A, Paker-Krush Y, Roussay-Maggi C, inventors; Selene Therapeutics Ltd., assignee. Brain Permeable DHODH Inhibitors and Uses Thereof. World Intellectual Property Organisation patent WO2025041128A1. 2025 Feb 27.

Popova G. Dihydroorotate Dehydrogenase: New Insights into an Old Target [dissertation]. Sweden: Karolinska Institutet; 2020.

Qu H, Wang S, He M, Wu Y, Yan F, Liu T, et al. Is it feasible to use AI-based drug design methods in the process of generating effective COVID-19 inhibitors? A validation study using molecular docking, molecular simulation, and pharmacophore methods. J Biomol Struct Dyn. 2023;1(1):1–14. doi: 10.1080/07391102.2024.2445169.

Raymer B, Bhattacharya SK. Lead-like Drugs: A Perspective. J Med Chem. 2018;61(23):10375–84. doi: 10.1021/acs.jmedchem.8b00407.

Reis RAG, Calil FA, Feliciano PR, Pinheiro MP, Nonato MC. The dihydroorotate dehydrogenases: Past and present. Arch Biochem Biophys. 2017;632(1):175–91. doi: 10.1016/j.abb.2017.06.019.

Ripphausen P, Nisius B, Bajorath J. State-of-the-art in ligand-based virtual screening. Drug Discov Today. 2011;16(9):372–6. doi: 10.1016/j.drudis.2011.02.011.

Rosales-Hernández MC, Correa-Basurto J. The importance of employing computational resources for the automation of drug discovery. Expert Opin Drug Discov. 2015;10(3):213–9. doi: 10.1517/17460441.2015.1005071.

Rosander C, Hallböök T. Dravet syndrome in Sweden: a population-based study. Dev Med Child Neurol. 2015;57(7):628–33. doi: 10.1111/dmcn.12709.

Rouini M-R, Dibaei M, Ghasemian E. Pharmacokinetics and Bioequivalence Studies of Teriflunomide in Healthy Iranian Volunteers. Clin Pharmacol Drug Dev. 2020;9(3):341–5. doi: 10.1002/cpdd.725.

Ruiz-Moreno AJ, Cedillo-González R, Cordova-Bahena L, An Z, Medina-Franco JL, Velasco-Velázquez M. Consensus Pharmacophore Strategy For Identifying Novel SARS-Cov-2 Mpro Inhibitors from Large Chemical Libraries. J Chem Inf Model. 2024;64(6):1984–95. doi: 10.1021/acs.jcim.3c01439.

Rzagalinski I, Hainz N, Meier C, Tschernig T, Volmer DA. Spatial and molecular changes of mouse brain metabolism in response to immunomodulatory treatment with teriflunomide as visualized by MALDI-MSI. Anal Bioanal Chem. 2019;411(2):353–65. doi: 10.1007/s00216-018-1444-5.

Shmuely S, Sisodiya SM, Gunning WB, Sander JW, Thijs RD. Mortality in Dravet syndrome: A review. Epilepsy Behav. 2016;64(1):69–74. doi: 10.1016/j.yebeh.2016.09.007.

Singh A, Maqbool M, Mobashir M, Hoda N. Dihydroorotate dehydrogenase: A drug target for the development of antimalarials. Eur J Med Chem. 2017;125(1):640–51. doi: 10.1016/j.ejmech.2016.09.085.

Sinha BK, Mason RP. Biotransformation Of Hydrazine Dervatives in the Mechanism of Toxicity. J Drug Metab Toxicol. 2014;5(3):168. doi: 10.4172/2157-7609.1000168.

Siraki AG. Chapter Two - Free Radical Metabolites in Arylamine Toxicity. In: Fishbein JC, Heilman JM, editors. Advances in Molecular Toxicology, 1st ed. Netherlands: Elsevier; 2013. p. 39-82.

Styr B, Gonen N, Zarhin D, Ruggiero A, Atsmon R, Gazit N, et al. Mitochondrial Regulation of the Hippocampal Firing Rate Set Point and Seizure Susceptibility. Neuron. 2019;102(5):1009-1024.. doi: 10.1016/j.neuron.2019.03.045.

Tang Y, Moretti R, Meiler J. Recent Advances in Automated Structure-Based De Novo Drug Design. J Chem Inf Model. 2024;64(6):1794–805. doi: 10.1021/acs.jcim.4c00247.

Tiwari MK, Singh R, Singh RK, Kim I-W, Lee J-K. Computational Approaches For Rational Design Of Proteins With Novel Functionalities. Comput Struct Biotechnol J. 2012;2(3):e201204002. doi: 10.5936/csbj.201209002.

Uytterhoeven V, Kaempf N, Verstreken P. Mitochondria Re-set Epilepsy. Neuron. 2019;102(5):907–10. doi: 10.1016/j.neuron.2019.05.023.

Varytė G, Arlauskienė A, Ramašauskaitė D. Pregnancy and multiple sclerosis: an update. Curr Opin Obstet Gynecol. 2021;33(5):378–83. doi: 10.1097/GCO.0000000000000731.

Veber DF, Johnson SR, Cheng H, Smith BR, Ward KW, Kopple KD. Molecular Properties That Influence the Oral Bioavailability of Drug Candidates. J Med Chem. 2002;45(12):2615–23. doi: 10.1021/jm020017n.

von Spiczak S, Stephani U. Therapie des Dravet-Syndroms. Z Für Epileptol. 2019;32(2):107–15. doi: 10.1007/s10309-018-0236-4.

Wang R, Gao Y, Lai L. LigBuilder: A Multi-Purpose Program for Structure-Based Drug Design. Mol Model Annu. 2000;6(7):498–516. doi: 10.1007/s0089400060498.

Wang R, Luhua L, Wang S. Further development and validation of empirical scoring functions for structure-based binding affinity prediction. J Comput Aided Mol Des. 2002;16(1):11–26. doi: 10.1023/A:1016357811882.

Wheless J, Weatherspoon S. Use of Stiripentol in Dravet Syndrome: A Guide for Clinicians. Pediatr Neurol. 2025;162(1):76–86. doi: 10.1016/j.pediatrneurol.2024.10.015.

Wirrell EC, Laux L, Donner E, Jette N, Knupp K, Meskis MA, et al. Optimizing the Diagnosis and Management of Dravet Syndrome: Recommendations From a North American Consensus Panel. Pediatr Neurol. 2017;68(1):18–34. doi: 10.1016/j.pediatrneurol.2017.01.025.

Wolber G, Langer T. LigandScout: 3-D Pharmacophores Derived from Protein-Bound Ligands and Their Use as Virtual Screening Filters. J Chem Inf Model. 2005;45(1):160–9. doi: 10.1021/ci049885e.

Wu YW, Sullivan J, McDaniel SS, Meisler MH, Walsh EM, Li SX, et al. Incidence of Dravet Syndrome in a US Population. Pediatrics. 2015;136(5):e1310–5. doi: 10.1542/peds.2015-1807.

Yi H, Albrecht M, Pan F, Valkonen A, Rissanen K. Stacking of Sterically Congested Trifluoromethylated Aromatics in their Crystals – The Role of Weak F···π or F···F Contacts. Eur J Org Chem. 2020;2020(38):6073–7. doi: 10.1002/ejoc.202001008.

Yuan Y, Pei J, Lai L. LigBuilder 2: A Practical de Novo Drug Design Approach. J Chem Inf Model. 2011;51(5):1083–91. doi: 10.1021/ci100350u.

Zeng T, Zuo Z, Luo Y, Zhao Y, Yu Y, Chen Q. A novel series of human dihydroorotate dehydrogenase inhibitors discovered by in vitro screening: inhibition activity and crystallographic binding mode. FEBS Open Bio. 2019;9(8):1348–54. doi: 10.1002/2211-5463.12658.

Zhang L, Geohagen BC, Gavin T, LoPachin RM. Joint Toxic Effects of the Type-2 Alkene Electrophiles. Chem Biol Interact. 2016;254(1):198–206. doi: 10.1016/j.cbi.2016.06.014.

Zhou Y, Tao L, Zhou X, Zuo Z, Gong J, Liu X, et al. DHODH and cancer: promising prospects to be explored. Cancer Metab. 2021;9(1):22. doi: 10.1186/s40170-021-00250-z.

Zhu H, Zhang Y, Li W, Huang N. A Comprehensive Survey of Prospective Structure-Based Virtual Screening for Early Drug Discovery in the Past Fifteen Years. Int J Mol Sci. Multidisciplinary Digital Publishing Institute; 2022;23(24):15961. doi: 10.3390/ijms232415961.

Ziobro J, Eschbach K, Sullivan JE, Knupp KG. Current Treatment Strategies and Future Treatment Options for Dravet Syndrome. Curr Treat Options Neurol. 2018;20(12):52. doi: 10.1007/s11940-018-0537-y.

Zuberi SM, Wirrell E, Yozawitz E, Wilmshurst JM, Specchio N, Riney K, et al. ILAE classification and definition of epilepsy syndromes with onset in neonates and infants: Position statement by the ILAE Task Force on Nosology and Definitions. Epilepsia. 2022;63(6):1349–97. doi: 10.1111/epi.17239.

Zuo Z, Liu X, Qian X, Zeng T, Sang N, Liu H, et al. Bifunctional Naphtho[2,3-d][1,2,3]triazole-4,9-dione Compounds Exhibit Antitumor Effects In Vitro and In Vivo by Inhibiting Dihydroorotate Dehydrogenase and Inducing Reactive Oxygen Species Production. J Med Chem. 2020;63(14):7633–52. doi: 10.1021/acs.jmedchem.0c00512.

List of Publications and Abstracts

Dear Paula Zammit,

Thank you for having submitted the above abstract for the 83rd FIP World Congress of Pharmacy and Pharmaceutical Sciences 2025, to be held in Copenhagen, Denmark from 31 August to 3 September 2025.

On behalf of the Congress Programme Development Group, it is our great pleasure to inform you that the abstract(s) below **has/have been accepted for poster presentation.**

Abstract(s) accepted as poster

Title	Drug Design and Optimisation at the Dihydroorotate Dehydrogenase (DHODH) Receptor Using the Teriflunomide Scaffold as a Lead.
Paper Number	2777
Paper Status	Abstract - Accepted as Poster
Theme	SIG - New medicines
Presenting Author	Dr Claire Shoemake

L-Università ta' Malta | Faculty of Medicine & Surgery | Department of Pharmacy

Drug Design and Optimisation at the Dihydroorotate Dehydrogenase (DHODH) Receptor using the Teriflunomide Scaffold as a Lead.

Paula Zammit & Claire Shoemake

Department of Pharmacy, Faculty of Medicine and Surgery, University of Malta, Msida, Malta

email: paula.zammit.19@um.edu.mt, claire.shoemake@um.edu.mt

INTRODUCTION

Mouse studies show that DHODH inhibition is a novel route for the treatment of epilepsy. Teriflunomide has been identified as a potent DHODH inhibitor with poor intra-cerebral penetration due to high polarity.[1]

AIMS

To use the teriflunomide scaffold to identify DHODH inhibitors with improved non-polar characteristics, predisposing to better intracerebral penetration, by means of virtual screening and *de novo* drug design.

METHOD

Virtual Screening (VS)

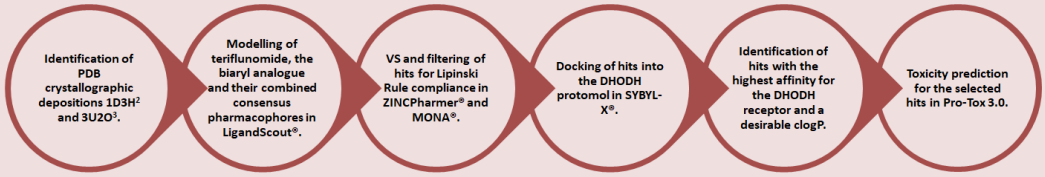

De novo design

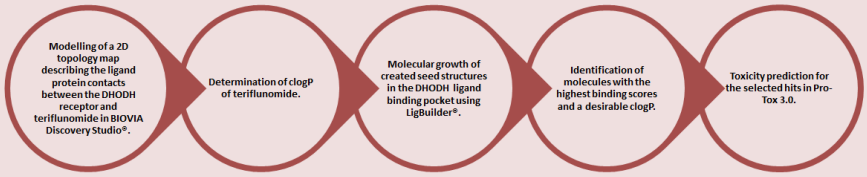

RESULTS

Virtual Screening: 299 Lipinski Rule compliant hits.

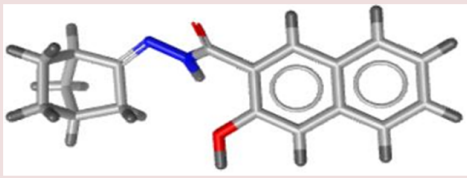

Figure 1.1: 3D structure of ZINC06536819, having the best properties of the VS cohort.

***De novo* design: 6 Lipinski Rule compliant hits.**

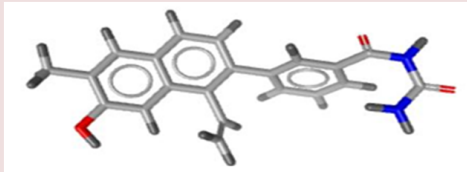

Figure 1.2: 3D structure of Seed30_Result195, having the best properties of the *de novo* cohort.

Table 1.1: Properties of the selected molecules.

	ZINC06536819	Seed30_Result19
clogP	3.45	4.96
Binding affinity	4.83 (Total Score)	8.45 (pKd)
Predicted toxicity class	4 (Harmful)	3 (Toxic)

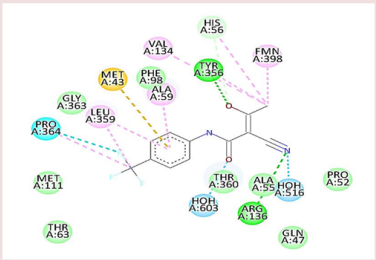

Figure 1.3: 2D topology map showing critical interactions between teriflunomide and the DHODH receptor.

CONCLUSION

The study produced molecules with improved non-polar characteristics (clogP of teriflunomide=2.13 vs. clogP of ZINC06536819=3.45 and clogP of Seed30_Result195=4.96), which predispose to increased intracerebral penetration. This allows the molecules to reach their site of the action in the brain and potentially exert an anti-epileptic effect. The VS molecules have affinities to the protomol and are more innovative than the *de novo* cohort. The *de novo* molecules have affinities to the ligand binding pocket and are more likely to be bioactive. All the molecules selected for further study require further optimisation to improve their toxicity profile and validation through molecular dynamics studies. The validated molecules can then be synthesized and tested *in vitro*.

REFERENCES

[1] Styr B, Gonen N, Zarhin D, Ruggiero A, Atsmon R, Gazit N et al. Mitochondrial Regulation of the Hippocampal Firing Rate Set Point and Seizure Susceptibility. Neuron. 2019;102(5):1009 1024. doi: 10.1016/j.neuron.2019.03.045.

[2] Liu S, Neidhardt E, Grossman T, Ocain T, Clardy J. Structures of human dihydroorotate dehydrogenase in complex with antiproliferative agents. Structure. 2000;8(1):25-33. doi: 10.1016/s0969-2126(00)00077-0.

[3] Erra M, Moreno I, Sanahuja J, Andrés M, Reinoso R, Lozoya E et al. Biaryl analogues of teriflunomide as potent DHODH inhibitors. Bioorg Med Chem Lett. 2011;21(24):7268-7272. doi: 10.1016/j.bmcl.2011.10.052.

Appendix 1

REDP Application ID MED-2024-00121

Current Status Acknowledged

If a submitted application needs to be amended, it can be withdrawn, edited, and resubmitted, and it will retain the same reference number. There is no need to submit a new application.